Molecular Therapy
Original Article

Therapeutic miR-21 Silencing Ameliorates Diabetic Kidney Disease in Mice

Malte Kölling,[1] Tamas Kaucsar,[4] Celina Schauerte,[1] Anika Hübner,[1] Angela Dettling,[1] Joon-Keun Park,[2] Martin Busch,[5] Xaver Wulff,[5] Matthias Meier,[2] Kristian Scherf,[1] Nóra Bukosza,[4] Gábor Szénási,[4] Mária Godó,[4] Amit Sharma,[6] Michael Heuser,[6] Peter Hamar,[4] Claudia Bang,[1] Hermann Haller,[2] Thomas Thum,[1,3,8] and Johan M. Lorenzen[1,2,7,8]

[1]Institute of Molecular and Translational Therapeutic Strategies (IMTTS), Hanover Medical School, 30625 Hannover, Germany; [2]Department of Nephrology, Hanover Medical School, 30625 Hannover, Germany; [3]National Heart and Lung Institute, Imperial College London, London SW3 6NP, UK; [4]Institute of Pathophysiology, Semmelweis University, 1085 Budapest, Hungary; [5]Department of Internal Medicine III/Nephrology, Jena University Hospital, 07747 Jena, Germany; [6]Department of Hematology, Hemostasis, Oncology and Stem Cell Transplantation, Hannover Medical School, 30625 Hannover, Germany; [7]Division of Nephrology, University Hospital Zürich, 8091 Zürich, Switzerland

Diabetic nephropathy is the main cause of end-stage renal disease. MicroRNAs are powerful regulators of the genome, and global expression profiling revealed miR-21 to be among the most highly regulated microRNAs in kidneys of mice with diabetic nephropathy. In kidney biopsies of diabetic patients, miR-21 correlated with tubulointerstitial injury. In situ PCR analysis showed a specific enrichment of miR-21 in glomerular cells. We identified cell division cycle 25a (Cdc25a) and cyclin-dependent kinase 6 (Cdk6) as novel miR-21 targets in mesangial cells. miR-21-mediated repression of Cdc25a and Cdk6 resulted in impaired cell cycle progression and subsequent mesangial cell hypertrophy. miR-21 increased podocyte motility by regulating phosphatase and tensin homolog (Pten). miR-21 antagonism in vitro and in vivo in streptozotocin-induced diabetic mice decreased mesangial expansion, interstitial fibrosis, macrophage infiltration, podocyte loss, albuminuria, and fibrotic- and inflammatory gene expression. In conclusion, miR-21 antagonism rescued various functional and structural parameters in mice with diabetic nephropathy and, thus, might be a viable option in the treatment of patients with diabetic kidney disease.

INTRODUCTION

Although diabetic nephropathy (DN) is the most common cause of end-stage renal disease (ESRD) in the Western world, its molecular mechanisms are still incompletely understood.[1] It involves various functional and structural renal changes, including renal hyperperfusion and filtration, mesangial matrix expansion and hypertrophy, basement membrane thickening, accumulation of extracellular matrix (ECM) proteins, and increased capillary permeability to diverse macromolecules, leading to progressive chronic kidney disease.[1] More than 40% of patients with diabetes eventually develop DN.[2] Moreover, DN is a strong risk factor for the development of various macrovascular complications, including atherosclerosis, hypertension, and stroke.[2,3] MicroRNAs (miRNAs) are under intense investigation as powerful regulators of various diseases with potential critical impact on disease initiation and/or progression, including diabetic kidney disease.[4] miRNAs represent small non-coding RNA transcripts with a length of ~22 nucleotides, that, through post-transcriptional binding of the 3′ UTR of mRNA targets, lead to the repression of gene and associated protein expression and/or translational inhibition of protein synthesis.[4] Intriguingly, a single miRNA may alter the expression of a large number of target genes, thus influencing a specific pathology by regulating whole disease-specific pathways and signaling cascades rather than a single gene. This unique function underlines the immense importance of these small molecules. miRNAs can be efficiently silenced in vivo by using specific miRNA antagonists.[4] Several miRNAs have been described to play a role in DN, including miR-192 and miR-21.[5,6] The role of miR-21 with regard to DN is still controversial. A previous study reported that genetic loss of miR-21 is associated with an aggravation of the disease process.[6] However, a recent study using a mouse model of Alport disease found pharmacological miR-21 silencing to result in a dramatic improvement of nephropathy progression by stimulating metabolic pathways.[7] In the present study, we identified miR-21 by global miRNA expression profiling as one of the major miRNAs upregulated in the kidneys of diabetic mice as well as in patients with DN. We describe novel targets of miR-21, including cell division cycle 25A (Cdc25a) and cyclin-dependent kinase 6 (Cdk6). In vivo treatment with a locked nucleic acid (LNA) targeting miR-21 ameliorated various functional parameters of DN, including tubulointerstitial fibrosis, mesangial matrix expansion, and albuminuria.

Received 10 January 2016; accepted 25 August 2016;
http://dx.doi.org/10.1016/j.ymthe.2016.08.001.

[8]These authors contributed equally to this work.

Correspondence: Johan M. Lorenzen, Division of Nephrology, University Hospital Zürich, Rämistrasse 100, 8091 Zürich, Switzerland.
E-mail: johan.lorenzen@usz.ch
Correspondence: Thomas Thum, Institute of Molecular and Translational Therapeutic Strategies (IMTTS), Hannover Medical School, Carl-Neuberg-Strasse 1, 30625 Hannover, Germany.
E-mail: thum.thomas@mh-hannover.de

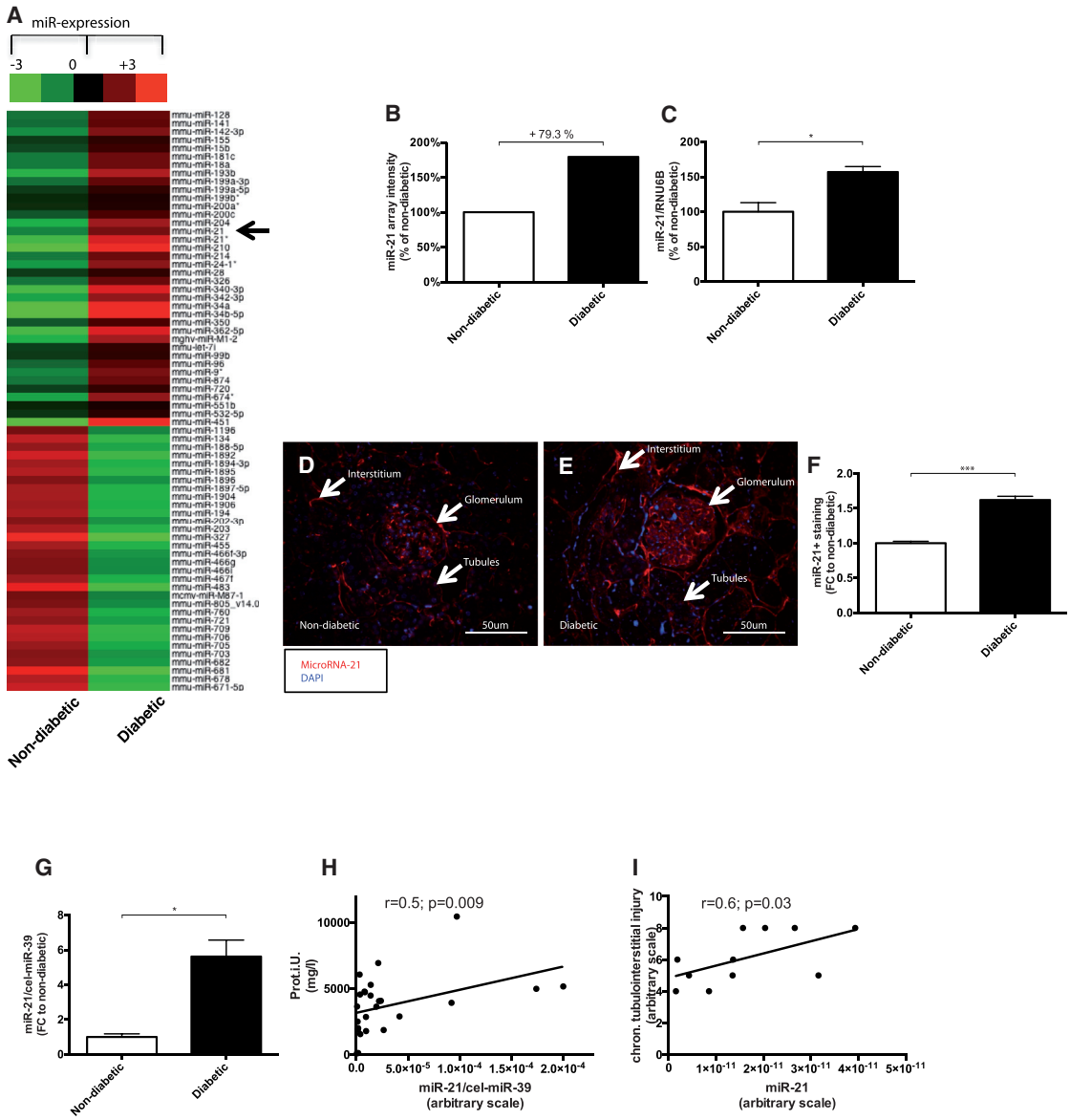

Figure 1. miR-21 in Diabetic Mice and Diabetic Patients

(A and B) miRNA-array analysis: arrow indicates miR-21 (A), miR-21 array quantification (B), and qPCR validation of miR-21 (C). miR-21 visualization by in situ PCR on kidney sections of non-diabetic (D) and diabetic (E) mice. (F) Quantification of in situ PCR miR-21 positive (red) staining. (G) Serum miR-21 expression is increased in diabetic patients compared to healthy controls. (H) Urinary miR-21 expression correlated with proteinuria in diabetic patients. (I) miR-21 expression in human kidney biopsies of diabetic patients correlated with chronic tubulointerstitial injury (percentage of injury was translated into the following arbitrary scale for further correlation studies: 1%–10% = 1; 11%–20% = 2; 21%–30% = 3; 31%–40% = 4; 41%–50% = 5; 51%–60% = 6; 61%–70% = 7; 71%–80% = 8; 81%–90% = 9; 91%–100% = 10) (I). *$p < 0.05$; **$p < 0.01$; ***$p < 0.001$; ****$p < 0.0001$.

Therefore, pharmacological silencing of miR-21 might be a novel efficient treatment strategy to halt the short- and long-term complications of DN.

RESULTS

miR-21 in Mice and Humans

In order to identify miRNAs that are critically involved in the development of diabetic kidney disease, we performed miRNA profiling in kidneys of healthy and streptozotocin-induced diabetic mice, which revealed several deregulated miRNAs in diabetic kidneys (Figure 1A). miR-21 was among the most highly upregulated miRNAs (Figures 1B and 1C). To investigate the specific localization of miR-21 upregulation in the kidney, we performed an in situ PCR on kidney sections of healthy and diabetic mice. In diabetic kidneys, miR-21 was enriched in all parts of the kidney, with the highest change in glomerular cells (Figures 1D–1F).

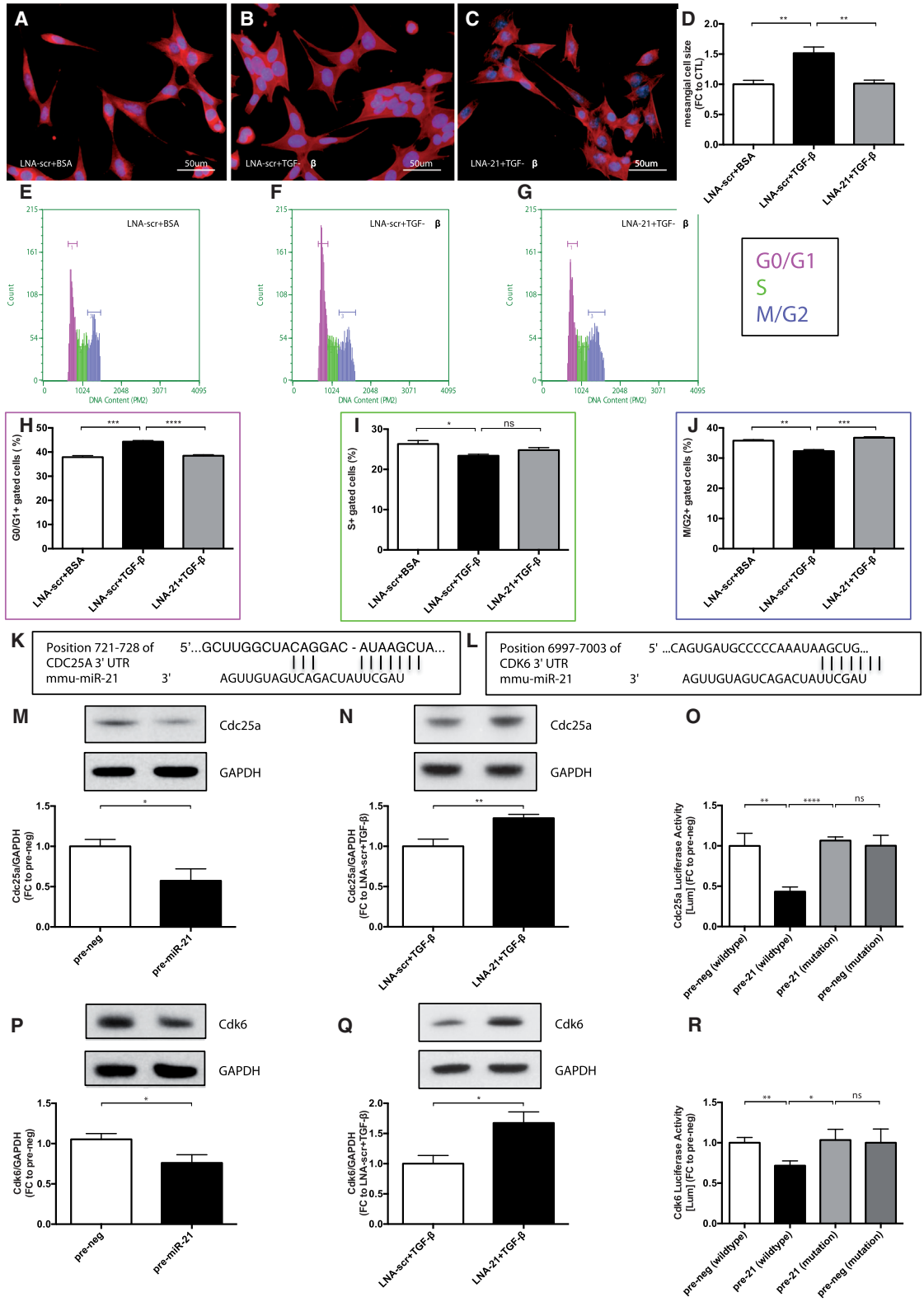

(legend on next page)

The plasma miR-21 concentration was increased in diabetic patients compared to healthy controls (Figure 1G). Furthermore, we show that urinary miR-21 correlated with proteinuria in patients (Figure 1H). We recently showed that urinary miR-21 concentration is increased in type II diabetic patients.[8] Interestingly, in patients with diabetic kidney disease we found a positive correlation of miR-21 expression with chronic tubulointerstitial injury in kidney biopsies (Figure 1I).

miR-21 Targets Cdc25a and Cdk6, Promoting Cell-Cycle Arrest in Mesangial Cells

Due to our findings by in situ PCR regarding the localization of miR-21 enrichment in DN, we evaluated the molecular mechanisms of miR-21 in mesangial cells (MCs). Transforming growth factor-β (TGF-β) is a major pro-fibrotic cytokine and has been shown to be strongly associated with kidney fibrosis under diabetic conditions.[9] TGF-β was significantly upregulated after treatment with advanced glycation end products (AGE-BSAs) in mesangial cells (Figure S1A). We thus used TGF-β in our in vitro studies. First, we found that the expression of miR-21 was significantly increased in MCs treated with TGF-β (Figure S1B). MC size was increased by TGF-β treatment compared to control treatment (Figures 2A, 2B, and 2D). Increased MC size by TGF-β was normalized by transfection with locked nucleic acids targeting miR-21 (LNA-21) as compared to LNA targeting a scrambled sequence (LNA-scr), suggesting a crucial role of miR-21 in MC hypertrophy (Figures 2C and 2D).

Long exposure to high glucose or TGF-β treatment arrested MCs in the G1-phase of the cell cycle and subsequently lead to MC hypertrophy.[10] We thus assessed whether inhibition of miR-21 prevents cell-cycle arrest in the G1-phase. TGF-β treatment of MCs confirmed cell-cycle arrest in G1 (Figures 2E, 2F, and 2H) and reduced proliferation (Figure S1C). Remarkably, silencing of miR-21 rescued the TGF-β-induced cell-cycle arrest in G1 (Figures 2G and 2H). In addition, the number of MCs treated with TGF-β was less in S- and M/G2-phase, respectively (Figures 2E, 2F, 2I, and 2J). Inhibition of miR-21 abrogated the TGF-β-mediated decrease of MCs in M/G2-phase (Figures 2G and 2J). These results propose miR-21 as a key regulator of cell cycle progression and prompted us to further investigate targets of miR-21. Using several bioinformatic algorithms to detect predicted targets of miR-21 that are involved in cell-cycle regulation, we identified Cdc25a and Cdk6 (Figures 2K and 2L). Cdc25a is important for the activation of cyclin-dependent kinases (Cdks).[11] Cdk6 is essential for cell cycle progression and G1/S transition.[12] Consequently, we show here that silencing of Cdc25a or Cdk6 by small interfering RNA (siRNA) resulted in G1-phase arrest of the cell cycle (Figures S2C–S2H). siRNA treatment resulted in a decrease of Cdc25a or Cdk6 by ∼50% (Figures S2A and S2B). To confirm the critical roles of Cdc25a and Cdk6 in cell-cycle regulation and cell proliferation, we overexpressed these targets in MCs by adenoviral vector transduction. MCs overexpressing Cdc25a and Cdk6 were detected to a lesser degree in G0/1 phase and more in S-phase (Figures S3A–S3C). Furthermore MCs overexpressing Cdc25a and Cdk6 showed significantly increased proliferation levels (Figures S3D and S3E). Next, the regulation of Cdc25a and Cdk6 by miR-21 was assessed on the protein level. Overexpression of miR-21 by transfection with precursor-miR21 (pre-miR-21) in comparison to a scrambled control (pre-neg) oligonucleotide showed significantly decreased Cdc25a and Cdk6 (Figures 2M and 2P) protein levels, whereas antagonizing miR-21 by transfection with LNA-21 in addition to TGF-β treatment significantly increased Cdc25a and Cdk6 (Figures 2N and 2Q) protein levels, supporting our hypothesis that Cdc25a and Cdk6 are direct targets of miR-21. To validate these results, we fused either the wild-type 3′UTR of Cdc25a and Cdk6 or the 3′UTR of both targets, in which the miR-21 binding sites were mutated, to a Luciferase reporter gene, respectively. Luciferase activity was significantly lower in pre-miR-21 transfected cells with constructs containing wild-type 3′UTR compared to transfection with pre-neg with wild-type 3′UTR and compared to pre-miR-21 and pre-neg transfected cells, in which the miR-21 binding sites in the 3′UTR were mutated (Figures 2O and 2R). Consequently, we identified Cdc25a and Cdk6 as novel and direct targets of miR-21, with a high impact on cell cycle progression and concomitant MC hypertrophy. Underlining our finding of cell-cycle arrest in G1, we found cyclin D1 protein degradation after TGF-β treatment (Figures S1M and S1N).

Regulation of Inflammation and Fibrosis in MC by miR-21

The expression of pro-fibrotic (TGF-β, Col1a2, fibronectin) as well as pro-inflammatory genes (monocyte chemoattractant protein-1 [MCP-1]) was increased in MCs subjected to AGE-BSAs (Figure S1A). Likewise, Col1a2, fibronectin, connective tissue growth factor (CTGF), and TGF-β itself were upregulated after TGF-β treatment (Figure S1D). To determine the relevance of miR-21 in fibrotic gene expression, we transfected MCs with precursor-miR-21 (pre-miR-21) or pre-negative control (pre-neg) oligonucleotides, locked nucleic acids targeting miR-21 (LNA-21), and additional TGF-β or locked nucleic acids targeting a scrambled sequence (LNA-scr) and additional TGF-β (Figures S1E and S1F). Increased expression of miR-21 resulted in upregulation of CTGF, MCP-1,

Figure 2. Mesangial Cell Hypertrophy Is Induced by miR-21-Mediated Repression of Cdc25a and Cdk6

(A and B) Mesangial cell hypertrophy displayed by F-actin staining (red) after transfection with LNA-scr and either BSA (A) as control (LNA-scr+BSA) or TGF-β (B) treatment (LNA-scr+TGFβ). (C) Inhibition of miR-21 by transfection of LNA-21 and additional TGF-β treatment (LNA-21+TGFβ). (D) Quantification of the cell size measurements (n = 5 each). (E–G) DNA histograms showing mesangial cells detected in G0/G1, S, or M/G2 phase of the cell cycle after LNAscr+BSA (E), LNA-scr+TGF-β (F), and LNA-21+TGF-β (G). (H–J) Quantification of cells detected in G0/G1 phase (H), S phase (I), and M/G2 phase (J) (n = 4). (K and L) Predicted consequential pairing of Cdc25a target region and miR-21 (K) and of Cdk6 target region and miR-21 (L), respectively (http://www.targetscan.org). (M and P) Western blot (WB) analysis of cytosolic Cdc25a (M) and Cdk6 (P) after overexpression of miR-21 by transfection with precursor-miR21 (pre-miR-21) in comparison to a scrambled control (pre-neg) oligonucleotide (n = 3). (N and Q) Western blot (WB) analysis of cytosolic Cdc25a (N) and Cdk6 (Q) after LNA-scr+TGFβ and LNA-21+TGFβ (n = 3). (O and R) Validation of miR-21 targeting Cdc25a (O) and Cdk6 (R) by Luciferase activity in relation to β-galactosidase activity after overexpression of miR-21 by transfection with pre-miR-21 in comparison to pre-neg with either wild-type or mutated target sites of Cdc25a and Cdk6 (n = 3). *p < 0.05; **p < 0.01; ***p < 0.001; ****p < 0.0001.

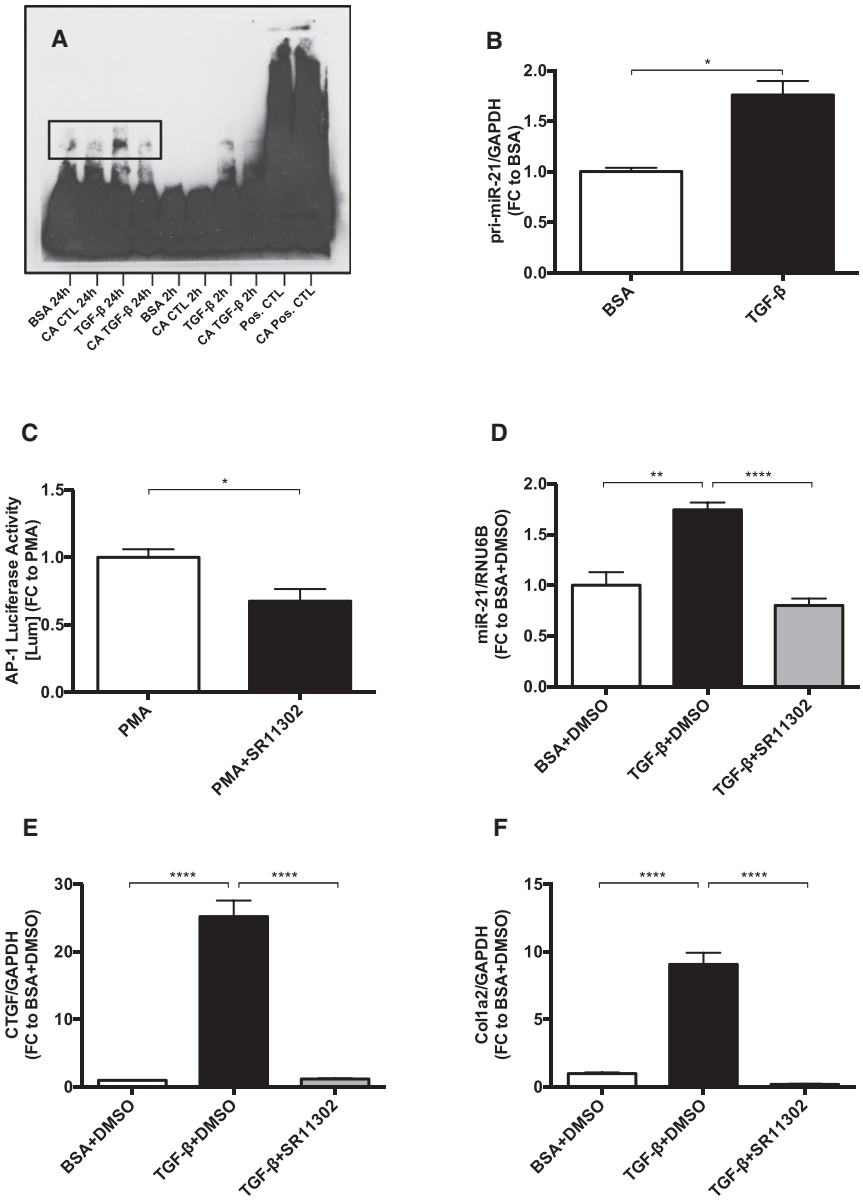

Figure 3. AP-1 as Key Transcriptional Activator of miR-21 in Mesangial Cells

(A) Electrophoretic mobility shift assay showing AP-1 activation as an AP-1/DNA complex (shifted band) after TGF-β treatment for 2 hr and 24 hr. (B) Every treatment was assessed in comparison to a competition assay (CA), respectively. qPCR quantification of primary-miR-21 after TGF-β treatment (n = 3). (C) AP-1 Luciferase activity in relation to β-galactosidase activity after an initial increase of AP-1 activity by phorbol myristate acetate (PMA) and subsequent AP-1 inhibition by synthetic retinoid 11302 (SR11302) (n = 4). (D–F) qPCR quantification of miR-21 (D), CTGF (E), and Col1a2 (F) after co-treatment with TGF-β and SR11302 (n = 4). *p < 0.05; **p < 0.01; ***p < 0.001; ****p < 0.0001.

and interleukin-6 (IL-6) (Figure S1G), whereas inhibition of miR-21 was highly protective against TGF-β-mediated upregulation of TGF-β, MCP-1, and IL-6 (Figure S1H). Investigating possible signaling pathways, we found that AKT and ERK were highly phosphorylated upon TGF-β treatment in MCs (Figures S1I–S1L).

AP-1 as Key Transcriptional Activator of miR-21

Electrophoretic mobility shift assay (EMSA) analysis showed that the transcription factor AP-1 was highly activated after TGF-β treatment (Figure 3A). We also detected an increase of primary miR-21 (pri-miR-21) after TGF-β treatment (Figure 3B), further suggesting transcriptional activation of miR-21 by TGF-β. To test whether inhibition of AP-1 has an impact on miR-21 expression, we used the AP-1 inhibitor synthetic retinoid SR11302. A functional concentration was determined by fusing AP-1 to a Luciferase reporter gene. The base level of AP-1 was increased by phorbol myristate acetate, a known activator of AP-1. 10 μM of SR11302 significantly decreased Luciferase activity (Figure 3C) and was thus used as a functional concentration for AP-1 inhibition. The inhibition of AP-1 by SR11302 rescued the TGF-β-induced upregulation of miR-21, proposing AP-1 as a key transcriptional activator of miR-21 (Figure 3D). We previously demonstrated by chromatin immunoprecipitation (ChIP) analysis using miR-21 promoter primers encompassing the AP-1 binding site that, indeed, AP-1 leads to transcription of miR-21.[13] Interestingly, the increased expression levels of CTGF and Col1a2 in MCs treated with TGF-β were also normalized by inhibition of AP-1 (Figures 3E and 3F).

miR-21 Induces Podocyte Motility

Podocyte dysfunction is one of the hallmarks of diabetic nephropathy.[14] In vitro, we found an increased expression level of miR-21 and Col1a2 in podocytes subjected to TGF-β (Figures 4A and 4B). To test, whether miR-21 is involved in podocyte dysfunction, we overexpressed and silenced miR-21 in podocytes. Overexpression of miR-21 increased podocyte migration, whereas inhibition of miR-21 reduced podocyte migration (Figures 4C–4H). Silencing of miR-21 enhanced protein levels of phosphatase and tensin homolog (Pten), identifying Pten as a bioinformatically predicted (miRTaBase) and experimentally validated target of miR-21 in podocytes (Figures 4I–4K). To confirm the functional role of Pten on podocyte motility, we developed a stable Pten overexpression podocyte cell line. We found that podocytes overexpressing Pten showed decreased migratory capacities (Figures S3F–S3H). Podocyte apoptosis was not affected by overexpression of miR-21 or inhibition of miR-21 under basal conditions (Figures 4L–4Q).

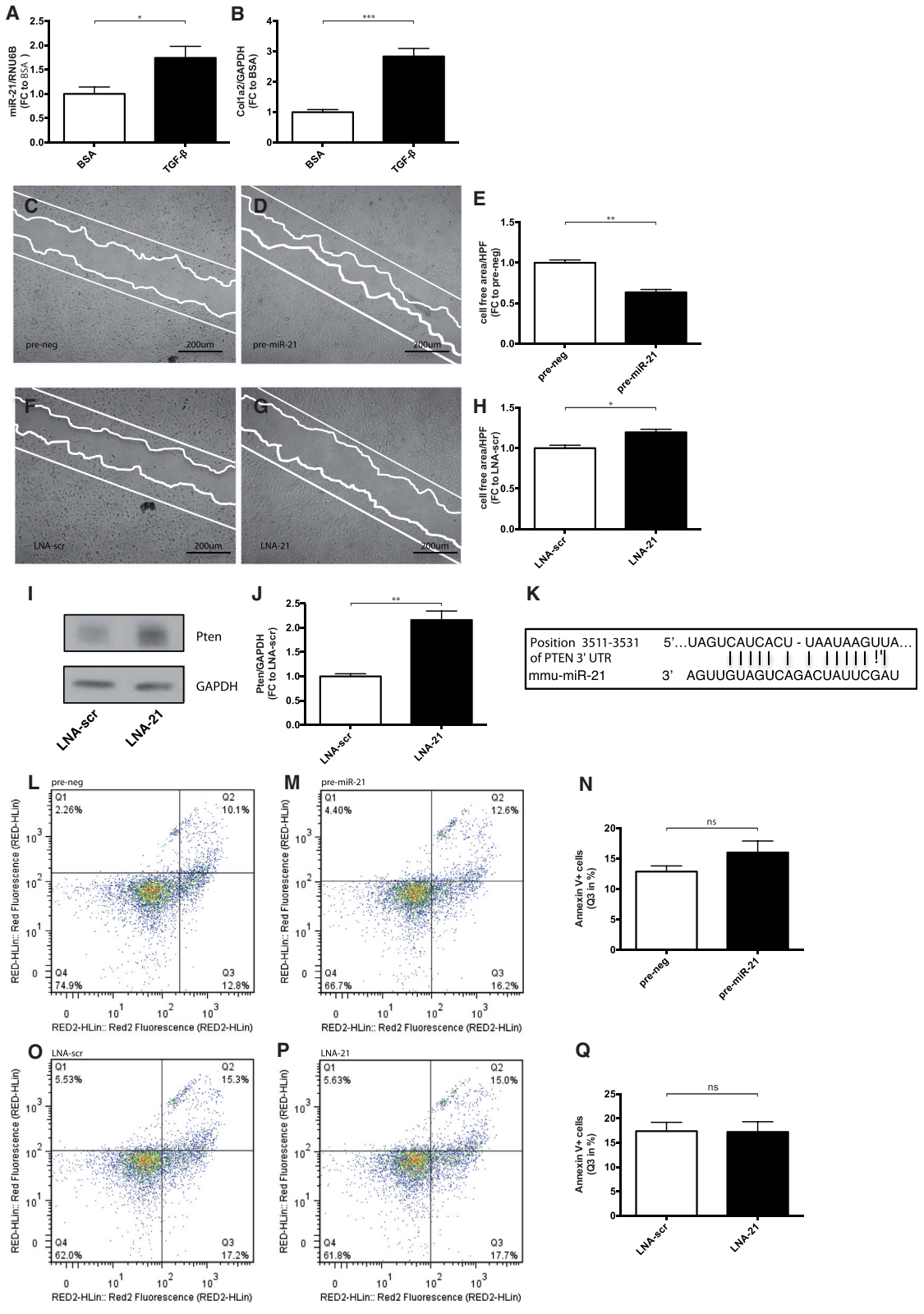

(legend on next page)

In Vivo Inhibition of miR-21 Reduces Diabetic Complications in Mice

Our aforementioned results strongly indicate miR-21 as a powerful regulator of mesangial cell hypertrophy and podocyte phenotype. Interestingly, antagonizing miR-21 in vitro prevented these detrimental events. We thus translated our in vitro findings to an in vivo molecular therapeutic approach in streptozotocin-induced diabetic mice by treating them with either LNA-21 or LNA-scr (see Figure S4A for efficacy of LNA-21 treatment; see Table 2 for animal characteristics).

In line with our in vitro findings, mesangial expansion was strongly reduced in mice treated with LNA-21, as assessed by periodic acid-Schiff (PAS) staining and subsequent mesangial index analysis (Figures 5A–D). Furthermore, development of interstitial fibrosis, as detected by Sirius Red staining, was significantly increased in the kidney sections of diabetic mice treated with LNA-scr, while LNA-21-treated mice were protected from collagen accumulation (Figures 5E–H). In addition, increased fibrotic gene expression (Col1a2, Col III, CTGF, and α-SMA) in DN was successfully rescued by miR-21 silencing (Figures 5N and 5O; Figures S4B and S4C).

The number of infiltrating F4/80$^+$ macrophages was significantly attenuated by LNA-21 treatment (Figures 5I–5L). Similarly, mice treated with LNA-21 were rescued from increased MCP-1 gene expression (Figure 5P), confirming our histological finding of reduced interstitial F4/80$^+$ macrophage infiltration (Figures 5I–5L).

Induction of DN resulted in a loss of intraglomerular WT-1$^+$ podocytes in LNA-scr-treated diabetic mice, while miR-21 silencing prevented podocyte loss (Figures 6A–6D). Streptozotozin treatment resulted in a reduction of podocyte numbers of ∼20% at week 8 of hyperglycemia (Figures 6A–6D). This is in line with previous reports.[15]

As mentioned above, Ccd25a and Cdk6 were identified as direct targets of miR-21. To verify in vivo relevance, we performed Cdc25a and Cdk6 immunofluorescence stainings on kidney sections. In line with our in vitro findings, we found reduced Cdc25a and Cdk6 signals in the diabetic group, while therapeutic inhibition of miR-21 rescued both the downregulation of Cdc25a and Cdk6 (Figures 6E–6L).

DN was associated with the development of albuminuria, as expected (Figure 5M). In line with a prevention of podocyte loss, albuminuria was significantly reduced in mice treated with LNA-21 as compared to mice treated with LNA-scr oligonucleotides (Figure 5M).

Glycated hemoglobin levels (HbA1c) of mice are shown in Figures S4D and S4E. LNA-21 treatment resulted in a small non-significant improvement of HbA1c levels.

DISCUSSION

In the present study, we found miR-21 to be increased in streptozotocin-induced diabetic mice through miRNA array analysis. Pharmacological silencing of miR-21 resulted in amelioration of various functional and structural parameters in streptozotocin-induced diabetic mice, including mesangial matrix expansion, tubulointerstitial fibrosis, inflammatory cell infiltration, albuminuria, and podocyte loss. miR-21 in situ PCR showed a marked enrichment of miR-21 in glomerular cells of mice upon diabetes induction. Moreover, we found miR-21 played a major role in patients with biopsy-proven diabetic kidney disease. miR-21 correlated with chronic tubulointerstitial injury and the degree of albuminuria. In addition, we show that miR-21 promotes a G1-phase arrest in MCs by regulating the novel targets Cdc25a and Cdk6, culminating in MC hypertrophy. The upstream transcription factor AP-1 was identified as a pivotal regulator of miR-21 expression. Furthermore, enhanced levels of miR-21 induced podocyte motility by regulating Pten. The main results of our study are summarized in Figure 7.

Several studies have examined the role of miRNAs in the pathogenesis of DN.[4–6] For instance, miR-192 mediates increases in the expression of collagen I in MCs.[5,16] The miR-29 family contributes to hyperglycemia-induced podocyte dysfunction[17] and progressive renal inflammation and fibrosis in type 2 diabetes.[18,19] The Let-7 as well as the miR-200 families are important regulators of renal fibrosis related to DN.[20–23] miR-21 has been demonstrated to amplify high glucose-induced mesangial cell pathology in vitro.[24] miR-21 in a mouse model of DN was recently shown to be associated with tubulointerstitial fibrosis by targeting SMAD7 and Pten.[25] We performed a whole genome miRNA expression analysis using pooled total RNA from kidneys of diabetic and non-diabetic mice. miR-21 was among the most highly regulated miRNAs in our analysis. Our miRNA deregulation differs slightly from previous analyses. This might be due to several reasons. In our experiments, a different strain of mice (SV129 mice in our study) was used, possibly leading to slight differences in results (as opposed to the C57BL/6J or DBA2J strains in previous analyses[5,16]). Another reason might be the fact that we investigated type I diabetic animals. Previous analyses focused on models of type II diabetes.[18] The pooling of RNA might also have impacted the results. However, we give strong evidence regarding the role of miR-21 in diabetic nephropathy. The analysis of the therapeutic potential of miRNA inhibition in vivo in DN is scarce. Here,

Figure 4. miR-21-Mediated Podocyte Phenotype

(A and B) qPCR quantification of miR-21 (A) and Col1a2 (B) after TGF-β treatment (n = 5). (C–H) Scratch migration for 8 hr in podocytes after pre-miR-21 treatment compared to pre-neg (C and D) and LNA-21 treatment compared to LNA-scr (F-G); quantification of the cell free area after 8 hr migration (E and H) (n = 6). (I and J) Western blot analysis of Pten after LNA-21 treatment compared to LNA-scr. (K) Predicted consequential pairing of Pten target region and miR-21 (miRTaBase). (L–Q) Annexin V apoptosis staining and FACS analysis of cells undergoing early apoptosis (quadrant 3 = Q3) after pre-miR-21 treatment compared to pre-negative controls (L–N) and LNA-21 treatment compared to LNA-scr (O–Q). RED fluorescence detects the level of cell viability using 7-amino actinomycin D (7-AAD), RED2 fluorescence represents annexin V positivity. *p < 0.05; **p < 0.01; ***p < 0.001; ****p < 0.0001.

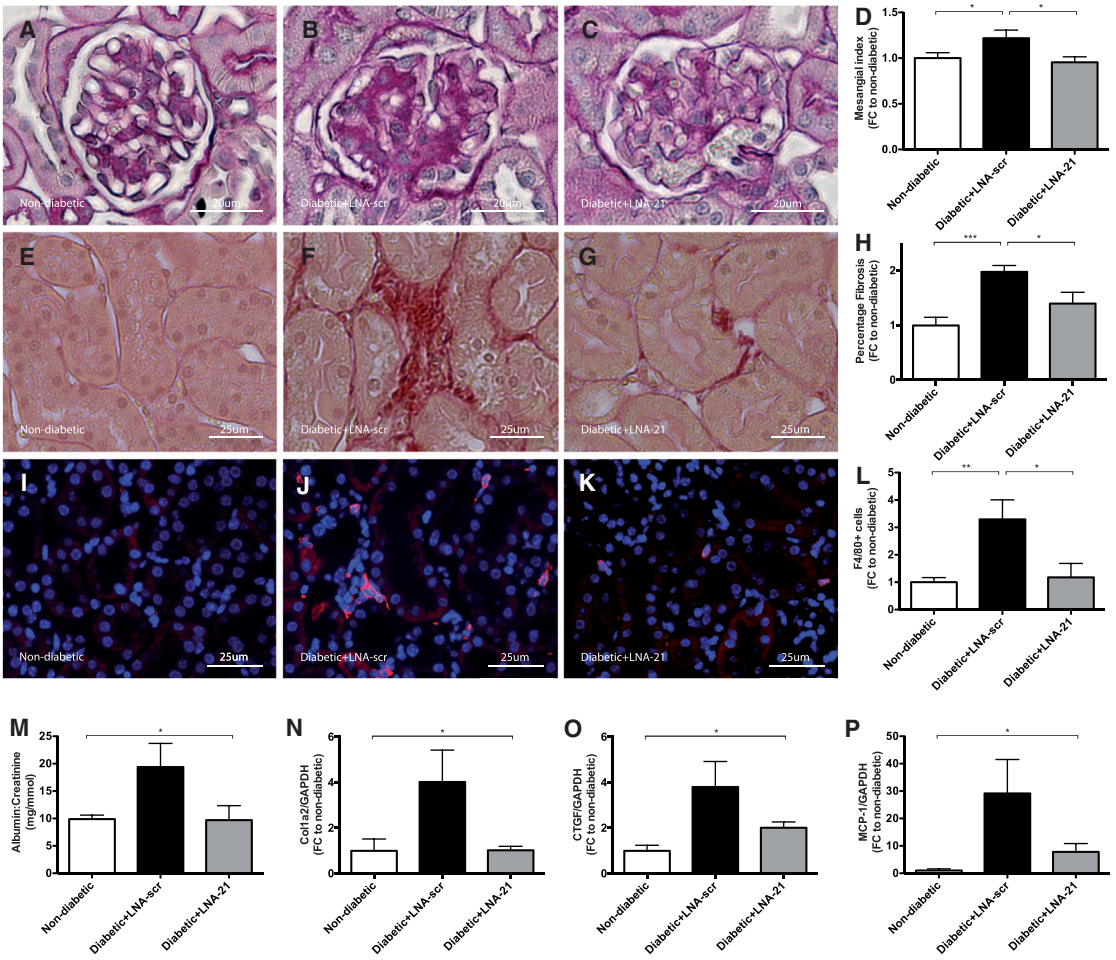

Figure 5. Molecular Therapeutic Inhibition of miR-21 Reduced Structural Complications in Diabetic Mice

Histological evaluation of therapeutic miR-21 inhibition in diabetic (STZ) mice. (A–D) Mesangial index analysis after periodic acid Schiff (PAS) staining in non-diabetic mice (A), diabetic mice with LNA-scrambled (B), and LNA-21 treatment (C) as well as quantification of results (D). (E–I) Detection of interstitial collagen by Sirius Red staining in non-diabetic mice (E), diabetic mice with LNA-scrambled (F), and LNA-21 treatment (G) as well as quantification of results (H). (I–L) Analysis of F4/80 (red) positive macrophage infiltration in non-diabetic mice (I), diabetic mice with LNA-scrambled (J), and LNA-21 treatment (K) as well as quantification of results (L). (M–P) Urinary albumin:creatinine ratio (M), qPCR quantification of Col1a2 (N), CTGF (O) and MCP-1 (P) in non-diabetic control mice as well as diabetic mice subjected to LNA-21 and LNA-scr treatment. Non-diabetic mice, n = 10. Diabetic (STZ) mice treated with LNA-scr, n = 6. Diabetic (STZ) mice treated with LNA-21, n = 5. *$p < 0.05$; **$p < 0.01$; ***$p < 0.001$; ****$p < 0.0001$.

we present a comprehensive analysis of the in vivo role of miR-21 in DN as well as the underlying mechanisms in different cellular compartments implicated in DN. In addition, we present evidence of the therapeutic potential of pharmacological miR-21 silencing in DN.

Contrary to our findings, genetic loss of miR-21 has recently been shown to aggravate the progression of DN in mice.[6] We found that diabetic miR-21-deficient TGF-β1-transgenic mice exhibited increased proteinuria and glomerular extracellular matrix deposition and podocyte loss. However, our results regarding the pharmacological silencing of miR-21 are strongly supported by the Duffield group,[7] which successfully silenced miR-21 in a genetic mouse model of Alport nephropathy, resulting in a dramatic improvement of survival and reduction of albuminuria, glomerulosclerosis, interstitial fibrosis, tubular injury, as well as inflammation. In fact, based on these results, a clinical phase I trial using miR-21 antagonists in healthy volunteers has already been completed and showed that the drug was well tolerated and did not show serious adverse events. A clinical phase II trial is now planned using miR-21 antagonists in patients with Alport syndrome. The difference between our study and the results of Lai et al.[6] regarding the role of miR-21 in DN might be due to the fact that genetic loss of miR-21 in the developing embryo might lead to phenotypic changes beyond context-specific alterations (diabetes) as opposed to the silencing of miR-21 in adult tissue. It is surprising that the silencing of miR-21 in vitro under basal conditions resulted in a significant increase in podocyte apoptosis in the study by Lai et al., because it is known that unchallenged miR-21 knockout animals do not have a pathological phenotype.[26] If miR-21 silencing

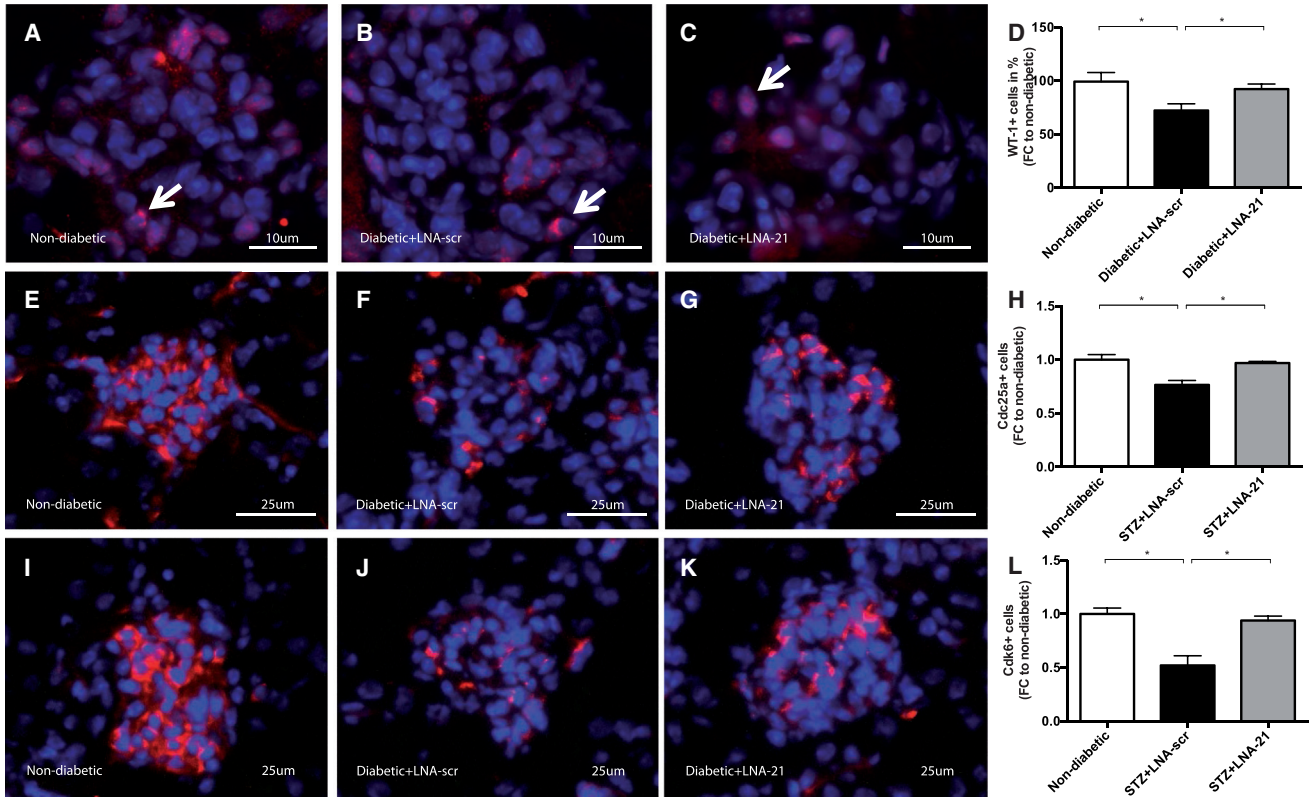

Figure 6. Molecular Therapeutic Inhibition of miR-21 Reduced Functional Complications in Diabetic Mice

(A–D) Determination of WT-1 (red) positive podocyte loss in non-diabetic mice (A), diabetic mice with LNA-scrambled (B), and LNA-21 treatment (C) as well as quantification of results (D). (E–H) Cdc25a immunofluorescence staining in non-diabetic mice (E), diabetic mice with LNA-scrambled (F), and LNA-21 treatment (G) as well as quantification of results (H). (I–L) Cdk6 immunofluorescence staining in non-diabetic mice (I), diabetic mice with LNA-scrambled (J), and LNA-21 treatment (K) as well as quantification of results (L). Non-diabetic mice, n = 10. Diabetic (STZ) mice treated with LNA-scr, n = 6. Diabetic (STZ) mice treated with LNA-21, n = 5. *$p < 0.05$; **$p < 0.01$; ***$p < 0.001$; ****$p < 0.0001$.

in otherwise unchallenged podocytes would result in apoptosis, it would be expected to also impact the phenotype of miR-21 knockout animals. In line with this, we did not detect an increase of podocyte apoptosis under basal conditions. In addition, in the study by Lai et al.,[6] TGF-β transgenic mice were crossed with miR-21 knockout animals. This highly artificial model may not reflect the in vivo situation seen in mice with diabetic nephropathy. On the contrary, the beneficial use of pharmacological miR-21 silencing has been demonstrated in various renal and extra-renal tissues, thus further supporting our findings. For instance, our group was able to demonstrate that miR-21 silencing in a mouse model of cardiac fibrosis resulted in a dramatic reduction of fibrosis.[13,27] Moreover, Duffield and co-workers underlined the efficacy of miR-21 silencing regarding fibrosis development in mice subjected to unilateral ureteral obstruction.[26] In renal fibrosis related to obstructive nephropathy or type II diabetes, miR-21 silencing has been successfully therapeutically applied.[28,29]

Based on our findings using the in situ PCR technique regarding the change of expression of miR-21 with diabetes induction, which mainly showed changes in the glomerular cells, we further characterized the functional role of miR-21 in vitro using MCs and podocytes.

MC hypertrophy is one of the earliest deteriorations in DN.[1,30,31] In the interphase of cellular growth, a G1 is separated from S and G2 phases.[30] Cells in the G1 phase of the cell cycle can further enter one of the following paths:[32] cells may (1) enter cell division, (2) undergo apoptosis, or (3) arrest at the G1/S transition, which causes an increase in cell size due to increases in the protein:DNA ratio (hypertrophy). Cell cycle progression is positively regulated by cyclins in complex with cyclin-dependent kinases.[32] Here, we introduce a novel mechanism of cell cycle disturbance by showing that miR-21 directly targets central positive regulators of G1/S-phase transition. Cdc25a is crucially involved in the activation of CDKs.[11] Additionally, miR-21 represses Cdk6, an essential contributor to cell cycle progression.[12] We also demonstrate that silencing of miR-21 targets Cdc25a and Cdk6, which results in G1-phase arrest, while viral overexpression promotes cell cycle progression, further underlining their importance. Taken together, our study indicates that the degradation of

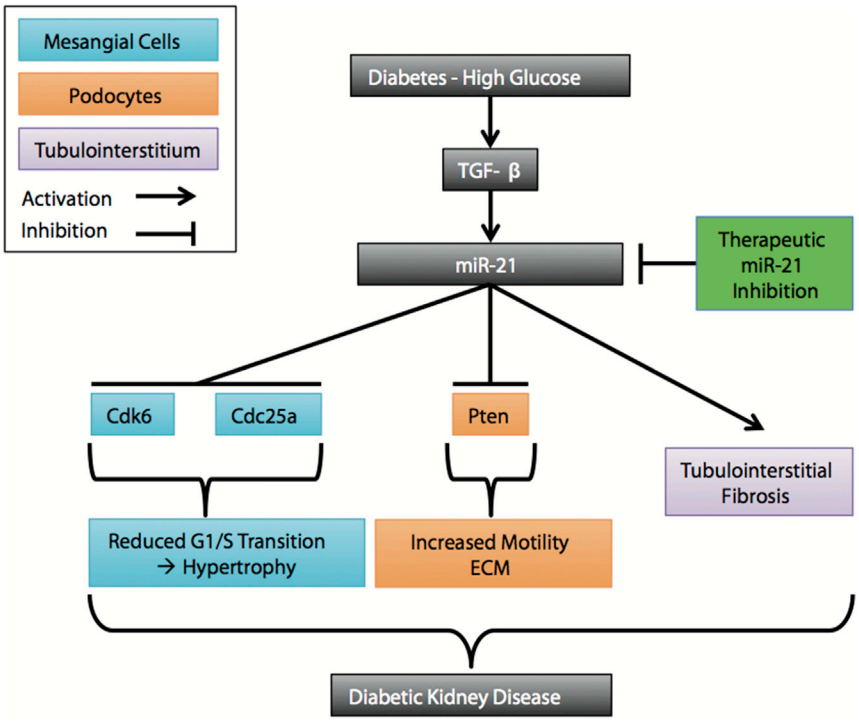

Figure 7. Summary of the Main Results
High glucose under diabetic conditions leads to an increase in TGF-β. miR-21 targets Cdc25a and Cdk6 in mesangial cells (turquoise), leading to mesangial cell hypertrophy by inducing a G1-phase arrest. miR-21 targets Pten, leading to increased podocyte motility and extracellular matrix production (orange). miR-21 leads to extracellular matrix accumulation (purple). These mechanisms contribute to diabetic kidney disease. miR-21 silencing ameliorates these phenomena.

two proteins, necessary for G1/S phase transition, finally results in MC hypertrophy in vitro and in vivo. This is the first report showing that Cdc25a and Cdk6 are targeted by miR-21 in MCs under diabetic conditions. Cdc25a has previously been identified to be targeted by miR-21 in colon cancer cells.[33] Moreover, we show that CTGF is regulated by miR-21 and that AKT signaling is activated by TGF-β. Previous reports show that CTGF reduced G1/S-phase transition[34] and that activation of AKT signaling lead to MC hypertrophy,[35] further supporting our findings.

Inflammation is another important mechanism in MCs. IL-6 is associated with mesangial expansion in diabetic patients.[36,37] We demonstrate that overexpression of miR-21 enhanced both IL-6 and MCP-1 expression. Thus, we propose that miR-21 is crucially involved in pro-inflammatory processes in MCs. Inflammation as well as pro-fibrotic processes were rescued by miR-21 silencing. This is in line with an amelioration of inflammatory gene expression as well as macrophage infiltration in whole kidneys of mice by miR-21 silencing in our study. The main findings in MCs are summarized in Figure S5.

Podocytes are functionally and structurally injured in the diabetic state.[14] Here, we show that miR-21 is crucially involved in podocyte motility by regulating Pten. We demonstrate that podocytes stably overexpressing Pten exhibit decreased migratory capacity, further underlining its importance for podocyte biology. miR-21-mediated podocyte motility suggests that miR-21 might be involved in enhanced leakiness of the slit diaphragm contributing to albuminuria. In vivo, therapeutic inhibition of miR-21 prevented podocyte loss and albuminuria, underlining the beneficial effects of an anti-miR-21 therapeutic strategy in podocytes. These findings are in line with Lin et al.,[38] indicating that Pten inhibition stimulates podocyte cytoskeletal rearrangement, leading to albuminuria. Moreover, Pten overexpression in podocytes has been shown to result in normalization of high glucose-induced phenotypic transitions and prevention of nephrin loss.[39]

Although several advances in the treatment of DN have been initiated, including effective blood pressure and blood glucose control, DN and its complications still pose a major risk factor for the development of end stage renal disease. By antagonizing miR-21 in vivo, we found several functional and structural parameters in DN to be successfully ameliorated.

In conclusion, our results described herein reveal that miR-21 is an important regulator of DN progression. miR-21 is mainly enriched in glomerular cells in DN, promoting cell-cycle arrest and subsequent MC hypertrophy by targeting Cdc25a and Cdk6 and leading to podocyte dysfunction by regulating Pten. Therapeutic miR-21 inhibition resulted in amelioration of various functional endpoints and is thus a promising future therapeutic in the treatment of patients with diabetic kidney disease. We administered LNAs targeting miR-21 at weeks 2 and 5. This is in line with a report showing that administration of a single dose of a locked nucleic acid targeting miR-21 results in a strong silencing of miR-21 in the kidney for at least 21 days.[40] Since 21 days is the latest time point assessed in this study, it can be inferred that miR-21 silencing is sustained for much longer periods of time. Several clinical trials involving miRNA-therapeutics have been or will be initiated: anti-miR-21 treatment in patients with Alport nephropathy, anti-miR-122 treatment in patients with hepatitis C virus infection, and anti-miR-221 treatment in patients with hepatocellular carcinoma. The emergence of these clinical trials underscores the potential therapeutic significance of anti-miR-strategies in the future routine treatment of patients. Our results regarding the successful use of miR-21 silencing in a murine model of DN suggest that miR-21 antagonism might be a viable therapeutic option in future clinical trials involving patients with DN.

Table 1. Demographic and Clinical and Laboratory Characteristics of Patients

	Total	Male	Female
Number of patients (n) (%)	26	20 (77)	6 (23)
Age (years)	63.2 ± 2.1	64.7 ± 2.5	58.2 ± 4.2
Serum creatinine (umol/L)	246.7 ± 30.8	256.6 ± 37.4	213.8 ± 50.3
GFR (mL/min/m^2)	31.0 ± 3.3	30.6 ± 3.7	32.2 ± 8.2
MAD (mm Hg)	103.8 ± 1.6	103.2 ± 1.9	105.7 ± 3.5
C-reactive protein (mg/L)	13.9 ± 4.1	14.0 ± 5.2	13.9 ± 4.8
Proteinuria (g/L)	3.1 ± 0.4	2.7 ± 0.4	4.8 ± 0.15
Concomitant Drug Treatment			
ARB (n) (%)	16 (62)	12 (46)	4 (15)
ACE inhibitors (n) (%)	14 (54)	12 (46)	2 (8)
Beta-blocker (n) (%)	22 (85)	18 (69)	4 (15)
Calcium channel blocker (n) (%)	22 (85)	17 (65)	5 (19)
Loop diuretics (n) (%)	23 (88)	19 (35)	4 (15)
Statins (n) (%)	17 (65)	14 (54)	3 (12)
Aspirin (n) (%)	14 (54)	12 (46)	2 (8)
Insulin (n) (%)	13 (50)	12 (46)	1 (4)
Metformin (n) (%)	3 (12)	3 (12)	0 (0)
Glimepiride (n) (%)	5 (19)	2 (8)	3 (12)
ESA (n) (%)	3 (12)	3 (12)	0 (0)

ARB, angiotensin receptor blocker; ACE inhibitor, angiotensin converting-enzyme inhibitor; ESA, erythropoietin stimulating agent; GFR, glomerular filtration rate; MAD, mean arterial pressure. Data are presented as mean ± SEM.

MATERIALS AND METHODS

Patients

Patient characteristics are described in Table 1. The ethical committee of the University Hospital Jena approved the study. 26 patients and 20 age-matched healthy controls were included. The diagnosis of diabetic nephropathy (or diabetic kidney disease [DKD]) was histologically confirmed after kidney biopsy in 11 patients. Biopsies were evaluated by an experienced renal pathologist, including the quantification of chronic tubular damage of the renal cortex in percent.

Animal Studies

Male SV129 mice (Charles River) were housed under standard conditions. Mice 8- to 10-weeks old and weighing between 20 and 30 g were used for all experiments. All procedures were carried out according to guidelines from the American Physiological Society and were approved by local authorities. All animal experiments were performed at Semmelweis University. The animals received a standard diet with free access to tap water. The Low-Dose Streptozotocin Induction Protocol according to the Animal Models of Diabetic Complications Consortium (AMDCC) was used. Weight-matched mice were fasted for 4 hr prior to injection. Mice then received 50 mg/kg body weight streptozotocin (STZ) (Sigma-Aldrich) in 100 mmol/L sodium citrate (pH 4.5) or sodium citrate buffer (control, n = 10) intraperitoneally for 5 consecutive days. Glucose levels from tail blood were measured with the glucometer Elite (Bayer) every day. Animals with glucose levels > 16 mmol/L on two consecutive measurements were regarded as hyperglycemic, and glucose measurements were extended to once weekly. Body weight was assessed at baseline and weekly during the course of the study. The mice received no insulin within the complete study period. Ketonuria did not occur (data not shown). Urine samples were taken every week to determine albuminuria levels as described previously.[41] After 8 weeks of hyperglycemia, the animals were sacrificed according to the following protocol. After anesthesia with avertin (2.5%), a laparotomy was performed, and urine was collected by puncturing the bladder with a 23-gauge needle. The abdominal aorta was canulated with a 23-gauge needle, and the organs were perfused with lactated Ringer solution. Table 2 shows animal characteristics.

LNA-Modified miRNA Oligonucleotides

The oligonucleotides were provided by Exiqon. Mice (n = 5 in LNA-21 STZ group, n = 6 in LNA-scr STZ group) were treated intraperitoneally with either locked nucleic acids targeting miR-21 (LNA-21) or targeting a scrambled mismatch sequence (LNA-scrambled) at a dose of 20 mg/kg body weight each at weeks 2 and 5 after STZ injection.

miRNA Global Transcriptome Analysis

miRNA expression analysis was performed in kidneys of diabetic and non-diabetic wild-type mice. Pooled total RNA from five mice with DN and five healthy control mice was used for genome-wide miRNA array analysis. The Affymetrix miRNA Gene- Chip array analysis was used according to the manufacturer's instructions (Affymetrix). The Cluster Gene 3.0 Program was used for analysis. Data was log transformed and genes and arrays were centered. Genes and arrays were finally clustered by Spearman rank correlation and average linkage.

miRNA and RNA Isolation and miRNA and mRNA RT-PCR

RNA isolation was performed with peqGold Trifast (VWR Peqlab) according to the manufacturer's instructions. For detection of miRNAs in samples, TaqMan miRNA assays (Applied Biosystems) were applied. RNU-6B was amplified as a control. RT-PCR analysis was performed (ICycler, Bio-Rad). Amplified cDNA was used as a template for qPCR (ViiA 7 Real-Time PCR System, Life Technologies). For detection of mRNAs in samples, RT was performed with total RNA using oligoDT primers (Bio-Rad). Amplified cDNA was used as a template for qPCR. qPCR analysis was performed (CFX96 Touch Real-Time PCR Detection System, Biorad) with iQ^{TM} SYBR Green Supermix (Biorad). The primers used in our study are depicted in Table S1.

miRNA-21 In Situ PCR

Sections (4 μm in thickness) from 4% paraformaldehyde (PFA)-fixed and paraffin-embedded kidney tissue were deparaffinized and digested with pepsin (Dako, Agilent Technologies) dilution for 20 min. The sections were treated with DNase I (Roche) overnight. Afterward, the tissue section was covered with the miRNA PCR

Table 2. Animal Characteristics: Glycemia, Glucosuria, and Body Weight

Mice	Week 0	Week 1	Week 2	Week 3	Week 4	Week 5	Week 6	Week 7	Week 8
Glycemia (mmol/L)									
Non-diabetic	6.8 ± 1.2	6.7 ± 1.0	6.7 ± 0.6	6.4 ± 0.7	6.2 ± 0.6	6.4 ± 1.2	5.7 ± 1.2	5.4 ± 0.6	5.9 ± 0.8
Diabetic+ LNA-scr	18.5 ± 1.5	19.5 ± 2.6	22.7 ± 2.0	24.5 ± 2.4	21.8 ± 2.3	22.8 ± 2.6	23.5 ± 2.5	23.3 ± 4.2	22.5 ± 3.1
Diabetic+ LNA-21	17.9 ± 1.2	21.2 ± 2.1	20.8 ± 2.4	20.0 ± 4.4	19.8 ± 3.8	18.4 ± 3.9	20.8 ± 2.6	20.0 ± 1.5	21.1 ± 5.0
p value[a]	0.45	0.26	0.19	0.06	0.19	0.05	0.11	0.17	0.57
Glucosuria (mmol/L)									
Non-diabetic	0.5 ± 0.3	–	–	–	0.4 ± 0.2	0.4 ± 0.2	0.4 ± 0.3	0.4 ± 0.1	0.4 ± 0.2
Diabetic+ LNA-scr	0.6 ± 0.4	–	–	–	74.4 ± 54.0	104.4 ± 41.7	116.4 ± 21.2	126.7 ± 2.9	127.5 ± 1.3
Diabetic+ LNA-21	0.9 ± 0.9	–	–	–	42.1 ± 49.0	55.7 ± 54.3	117.9 ± 13.8	101.7 ± 32.7	92.2 ± 40.9
p value[a]	0.52	–	–	–	0.33	0.13	0.90	0.09	0.06
Body Weight (g)									
Non-diabetic	25.4 ± 1.7	26.4 ± 1.5	27.3 ± 1.6	27.6 ± 1.3	27.8 ± 1.7	28.4 ± 1.5	27.6 ± 1.6	28.1 ± 1.9	28.4 ± 1.9
Diabetic+ LNA-scr	23.5 ± 1.7	23.6 ± 1.7	23.8 ± 1.6	23.3 ± 2.0	23.5 ± 2.0	23.9 ± 1.6	24.1 ± 2.2	24.1 ± 2.2	24.3 ± 2.0
Diabetic + LNA-21	24.5 ± 1.7	24.6 ± 1.5	24.3 ± 1.2	24.6 ± 1.0	24.64 ± 1.3	25.1 ± 1.4	24.8 ± 0.8	25.7 ± 1.5	26.0 ± 1.4
p value[a]	0.40	0.43	0.35	0.32	0.40	0.41	0.50	0.25	0.15

Data are presented as mean ± SD.
[a]LNA-scr versus LNA-21.

solution, consisting of miR-21 primers (RT: 5′-GTCGTATCCA GTGCAGGGTCCGAGGTATTCGCACTGGATACGACTCAACA; forward: 5′- TGCGGTAGCTTATCAGACTGA; reverse: 5′-GTGC AGGGTCCGAGGT), digoxigenin dUTP (Roche), RNase inhibitor (Roche), and SuperScript One-Step RT-PCR System with Platinum Taq DNA Polymerase (Life Technologies). The corresponding primer for cel-miR-39 (RT: 5′- GTCGTATCCAGTGCAGGGTCCGAGG TATTCGCACTGGATACGACCAAGCT; forward: 5′-GCCCTCA CCGGGTGTAAAT; reverse: 5′-GTGCAGGGTCCGAGGT) was used as negative control. cDNA synthesis was performed by incubating slides for 30 min at 60°C. Then cDNA was amplified after denaturing at 94°C for 4 min with 26 cycles at 94°C denaturation (15 s), 56°C annealing (30 s), and 72°C extension (20 s) followed by final extension at 72°C for 5 min. The digoxigenin-labeled miRNA cDNA was detected with a digoxigenin antibody (Roche).

Histology and Immunostaining

After kidney extraction, a representative part of each kidney was fixed immediately in PBS-buffered 4% paraformaldehyde and embedded in paraffin. Sections (4 μm in thickness) were used for immunostainings, periodic acid-Schiff (PAS), and Sirius Red stainings. PAS staining was used to evaluate mesangial expansion by mesangial index (MI) determination according to the protocol of the Animal Model of Diabetic Complications Consortium (AMDCC): area (pixel) of PAS staining / total area (pixel) of glomerulus. MI was examined in at least 30 glomeruli per animal. Collagen accumulation was assessed by Sirius Red staining: area (pixel) of Sirius Red staining / total kidney area (pixel), displayed in percentage of fibrosis. In vitro, mesangial hypertrophy was assessed by measuring cell size after phalloidin-TRITC (Sigma-Aldrich) staining F-actin in the cytoplasm of cells.

Immunostainings

Deparaffinized kidney sections were boiled in citrate buffer for antigen retrieval, blocked with 5% donkey serum, and incubated overnight at 4°C with primary antibodies. This was followed by antibody visualization using Alexa 488/Alexa 594 secondary antibodies (Molecular Probes/Invitrogen). Immunostainings for inflammatory cell influx was performed using the following primary antibody: monoclonal rat anti-mouse F4/80 (Serotec). Quantification of F4/80-expressing cells was performed by counting positive cells in five randomly chosen non-overlapping fields. Immunostainings for podocyte number per glomerular tuft were performed in frozen sections using the following primary antibody: polyclonal rabbit anti-mouse WT-1 (Santa Cruz Biotechnology). Here, podocyte density was assessed by counting at least 30 glomeruli of each section by nuclear (Dapi-staining) and podocyte (WT-1 staining) as described previously.[7] Immunostainings of miR-21 targets were performed in frozen sections using the following primary antibodies: monoclonal mouse anti-mouse/rat/human Cdc25a (Santa Cruz Biotechnology) and monoclonal mouse anti-mouse/rat/human Cdk6 (Abcam).

Cell Culture Experiments

For in vitro analyses, a mouse mesangial cell line and a WT5 podocyte cell line were used. Mesangial cells were cultured in DMEM (Life Technologies) supplemented with 10% FCS and 1% penicillin or streptomycin. For proliferation, the WT5 podocyte cell line was cultured under permissive conditions at 33°C with RPMI (Life Technologies) supplemented with 10% FCS, 1% penicillin or streptomycin, and 100 U/mL IFN-γ. For differentiation prior to experiments, the WT5 podocyte cell line was cultured under non-permissive conditions at 37°C with RPMI (Life Technologies) supplemented with

10% FCS, 1% penicillin or streptomycin and without IFN-γ. Cells were grown to 60% to 70% confluence and used for further downstream analyses. Cells were treated with TGF-β at a concentration of 4 ng/mL (mesangial cells) or 10 ng/mL (WT5 podocytes) or with advanced glycation end products at a concentration of 100 μg/mL (AGE-BSA, Millipore) for 24 hr. BSA is widely used as a carrier protein to enhance the stability of recombinant proteins. Thus, we decided to use BSA without TGF-β as the control treatment to eliminate possible effects of BSA itself.

Transfection Assays

Transient liposomal transfections with locked nucleic acids targeting miR-21 (LNA-21, Exiqon) or locked nucleic acids targeting a mismatch sequence (LNA-scrambled, Exiqon), precursor-miRNA-21 (pre-miR-21, Ambion) or pre-negative control (pre-neg, Ambion) oligonucleotides, as well as small interfering RNA (Santa Cruz Biotechnology) silencing Cdc25a, Cdk6, or a control siRNA were performed according to the manufacturers' instructions. Briefly, cells were split 1 day before transfection to reach 60% to 70% confluence on the day of transfection. Specific LNA-21/pre-miR-21 and scrambled controls (LNA-scr/pre-neg) and Lipofectamine 2000 (Invitrogen) were mixed separately and incubated for 5 min with Opti-MEM I media (Invitrogen). Complexes were added together and incubated for 20 min. Media were changed to antibiotic-free media before the addition of liposomal LNA/pre-miR complexes (final concentration 100 nmol/L). Cells were incubated for 4 hr before the media were changed to fresh media. Cells transfected with LNA were additionally treated with 4ng/mL TGF-β (mesangial cells) to mimic therapeutic effects under diabetic conditions or 0.1% BSA as control for the last 24 hr of transfection. Silencing or augmenting of miRNA targets was monitored after 48 hr of transfection by western blot analysis.

Protein Analysis

Western blot analysis was performed using 10 to 40 μg of total protein. Tissue was homogenized and cells were pelleted. Cell lysis was performed (cell lysis buffer, Cell Signaling Technology) and protein electrophoresis was initiated. Proteins were transferred to polyvinylidene difluoride (PVDF) membranes, blocked with 5% milk in TBS-Tween, and probed overnight at 4°C with the following primary antibodies: Cdc25a (rabbit anti-mouse/human, Abcam), Cdk6 (mouse anti-mouse/rat/human, Abcam), phospho-AKT (ser) (rabbit anti-mouse/rat/human, Cell Signaling Technology), AKT (rabbit anti-mouse/rat/human, Cell Signaling Technology), phospho-ERK (44/42) (rabbit anti-mouse/rat/human, Cell Signaling Technology), ERK (rabbit anti-mouse/rat/human, Cell Signaling Technology), CyclinD1 (mouse anti-mouse, Santa Cruz Biotechnology). Antibody binding was visualized by chemiluminescence (Super-Signal West Pico Chemiluminescent, Thermo Fisher Scientific). Rabbit anti-mouse glyceraldehyde 3-phosphate dehydrogenase (GAPDH; Sigma-Aldrich) was used as an internal loading control and for normalization of protein quantification. Immunoblots were scanned and quantified using ImageJ densitometry software.

MicroRNA Target Prediction

The microRNA databases and target prediction tools miRBase, DIANA-MICROT, MICRORNA.ORG, MIRDB, RNA22-MMU, and TARGETSCAN-VERT were used to identify potential microRNA targets.

Luciferase Reporter Assays

A luciferase reporter assay system was applied to validate potential miRNA targets as described previously.[42] A putative 3′UTR miRNA binding sequence was cloned into the *Spe*I and *Hind*III cloning site of pMIR-REPORT vector (Ambion): cell division cycle 25a (Cdc25a) wild-type: 5′-TCAGA…CTGAC**ATAAGCTA**AATC...TCCAT-3′; cyclin-dependent kinase 6 (Cdk6) wild-type: 5′-TCATT…CCCAA**ATAAGCT**GCATG...TCATG-3′. A mutation of the miR-21 binding site was also performed by gene synthesis of Cdc25a and Cdk6 3′UTR encompassing mutated target sequences of miR-21 by Eurofins Genomics: mutated cell division cycle 25a (Cdc25a): 5′-TCAGA…CTGAC**ATAGTATA**AATC...TCCAT-3′; mutated cyclin-dependent kinase 6 (Cdk6): 5′-TCATT…CCCAA**ATGGTCT**GCATG...TCATG-3′. These were also cloned into pMIR-REPORT vector (Ambion) between SpeI and HindIII sites. The resulting constructs were co-transfected with the miRNAs of interest and a β-galactosidase control plasmid (Promega) into HEK293 reporter cells in 48-well plates by use of Lipofectamine 2000 (Invitrogen). A total of 0.2 μg of plasmid DNA and 100 nmol/L miRNA was applied. Cells were incubated for 24 hr before luciferase and β-galactosidase activity was measured (Promega).

Cell Cycle Analysis

Labeling of cellular DNA with propidium iodide was performed to determine cells in different stages of the cell cycle using Guava Cell Cycle Reagent (Guava Technologies) according to the manufacturer's instructions. Cell cycle analysis was performed by fluorescence-activated cell sorter analysis (FACS) on a Guava easyCyte sorter (Millipore) using the Cytosoft software (Guava Technologies).

Proliferation Assay

Bromodeoxyuridine (BrdU) Cell Proliferation ELISA Kit (Abcam) was used to measure the proliferation rate. The assay was performed according to the manufacturer's instructions.

EMSA

EMSA "Gel Shift" Kit (Affymetrix) and EMSA Probe Set (Panomics) were used to detect transcriptional activation of AP-1 according to the manufacturer's instructions. In brief, EMSA is based on the separation of unbound DNA from AP-1/DNA complexes due to differences in electrophoretic mobility in native polyacrylamide gels. The gel is transferred to a nylon membrane and detected using strepatvidin-HRP and a chemiluminescent substrate. The shifted bands corresponding to the protein/DNA complexes are visualized relative to the unbound double-stranded DNA (dsDNA). For more specific binding, unlabeled specific dsDNA probe (competition assay) was added to the protein/DNA reaction

mixture, which competes with the labeled dsDNA probe (biotin-labeled probe) for binding to the protein. This causes the labeled probe to migrate to the bottom of the gel and reduces the intensity of the shifted band.

Transcriptional Activation Studies

Synthetic retinoid 11302 (SR11302, R&D Systems) was used to inhibit AP-1 activity. A functional concentration of SR11302 was determined by co-transfection of an AP-1 plasmid (4×AP-1 luciferase reporter plasmid [4×AP-1-Luc]) with a β-galactosidase control plasmid (Promega) into HEK293 reporter cells in 48-well plates by use of Lipofectamine 2000 (Invitrogen). The AP-1 plasmid (4×AP-1 luciferase reporter plasmid [4×AP-1-Luc]) was previously described.[42] In brief, the (AP-l)4-Luc contains four repeats (4×) of AP-1 binding sequences (TGAGTCA) under control of a luciferase reporter.[43] A total of 0.2 μg of plasmid DNA was applied. Additionally, the base level of AP-1 was increased by phorbol myristate acetate (PMA), a known activator of AP-1. Luciferase and β-galactosidase activity was measured (Promega) after 24 hr of transfection. An effective and significant reduction of Luciferase activity was reached with 10 μM of SR11302. Mesangial cells were co-treated with 4ng/mL TGF-β and 10 μM of SR11302 before miR-21, CTGF, and Col1a2 gene expression levels were determined by qPCR.

Scratch Wound Healing Assay of Podocytes

WT5 podocyte cell line was cultured under non-permissive conditions at 37°C with RPMI (Life Technologies) supplemented with 10% FCS, 1% penicillin or streptomycin and without IFN-γ. Transient liposomal transfection with pre-miR-21 or pre-neg was performed as described above. The scratches in the cell monolayer were generated with a 100 μL tip, and the cells were photographed after 0 and 8 hr of migration with a Nikon Ti 90 microscope. Subsequently, the cell-free area was calculated.

Annexin Apoptosis Assay

The detection of cells undergoing early apoptosis was performed by Annexin V and 7-amino actinomycin D (7-AAD) staining using the FlowCellectTM Annexin Red Kit (Millipore) according to the manufacturer's instructions. The analysis was performed by fluorescence-activated cell sorter analysis (FACS) on a Guava easyCyteTM sorter (Millipore) using the Cytosoft software (Guava Technologies).

Adenoviral Overexpression of Cdc25a and Cdk6 in Mesangial Cells

Cdc25a and Cdk6 adenoviral gene expression vectors (pAV[Exp]-CMV) were constructed by Vector Builder (Cyagen Biosciences). Adenoviral MC transduction was performed in the presence of protamine sulfate (4 ug/mL). The cells were infected with adenovirus vectors at an MOI of 50. Eight hours after transduction, the medium was changed to fresh medium. An adenovirus-expressing GFP (eGFP) was used as control. Downstream analyses were performed 48 hr after transduction.

Retroviral Overexpression of Pten in WT5 Podocytes

As previously described,[44] helper-free recombinant retrovirus produced in supernatants of transfected amphotropic Phoenix packaging cells was used to transduce WT5 podocytes.

Glycated Hemoglobin Count

Hemoglobin levels in blood samples taken at the study endpoint (8 weeks of hyperglycemia) were assessed by use of a mouse hemoglobin ELISA kit (Abcam). Glycated hemoglobin levels were analyzed by mouse ELISA (CrystalChem). Glycated hemoglobin levels are given as the percent of total hemoglobin count and in mmol/mol.

Statistical Analysis

Average data are presented as mean and SEM unless otherwise stated. All statistical analyses were performed with the SPSS package (SPSS, Inc.) and GraphPad Prism software (GraphPad Prism Software). Two-sided p values < 0.05 were considered statistically significant for all statistical procedures used. For the statistical comparison of two groups, we used an unpaired two-tailed Student t test; for the comparison of three or more groups, we used ANOVA followed by Tukey post hoc tests. In the figures, p values are indicated: *$p < 0.05$; **$p < 0.01$; ***$p < 0.001$; ****$p < 0.0001$.

SUPPLEMENTAL INFORMATION

Supplemental Information includes five figures and one table and can be found with this article online at http://dx.doi.org/10.1016/j.ymthe.2016.08.001.

AUTHOR CONTRIBUTIONS

A.S. and M.H. provided RSF91 dTomato control and RSF91 dTomato phosphatase and tensin homolog (Pten) retroviral plasmids. JML conceived and designed the experiments and wrote the paper. T.T., M.M., M.K., and H.H. wrote parts of the paper. C.B., A.D., A.H., K.S., and C.S. performed the in situ hybridization and helped with stainings of paraffin-embedded sections. J.K.P. analyzed histological stainings. M.B. and X.W. provided human samples. T.K., N.B., G.S., M.G., and P.H. performed the animal experiments. M.K. performed in vitro experiments and work-up of animal tissue.

ACKNOWLEDGMENTS

We thank Prof. Dr. H.-J. Gröne (German Cancer Research Center (DKFZ), Cellular and Molecular Pathology) for histopathologic diagnosis of kidney biopsies. This work was funded by a grant from the Else Kröner-Fresenius Foundation (to J.M.L. and T.T.), the Else Kröner-Fresenius Memorial scholarship (to J.M.L.), the REBIRTH Excellence Cluster (to T.T.), and the Integrated Research and Treatment Center Transplantation (IFB-Tx) (to T.T. and J.M.L.). T.T. received and licensed a miRNA-based patent about the use of miR-21 inhibitors in fibrotic diseases.

REFERENCES

1. Raptis, A.E., and Viberti, G. (2001). Pathogenesis of diabetic nephropathy. Exp. Clin. Endocrinol. Diabetes *109* (*Suppl 2*), S424–S437.

2. Fineberg, D., Jandeleit-Dahm, K.A., and Cooper, M.E. (2013). Diabetic nephropathy: diagnosis and treatment. Nat. Rev. Endocrinol. *9*, 713–723.

3. Sarnak, M.J., Levey, A.S., Schoolwerth, A.C., Coresh, J., Culleton, B., Hamm, L.L., McCullough, P.A., Kasiske, B.L., Kelepouris, E., Klag, M.J., et al.; American Heart Association Councils on Kidney in Cardiovascular Disease, High Blood Pressure Research, Clinical Cardiology, and Epidemiology and Prevention (2003). Kidney disease as a risk factor for development of cardiovascular disease: a statement from the American Heart Association Councils on Kidney in Cardiovascular Disease, High Blood Pressure Research, Clinical Cardiology, and Epidemiology and Prevention. Circulation *108*, 2154–2169.

4. Lorenzen, J.M., Haller, H., and Thum, T. (2011). MicroRNAs as mediators and therapeutic targets in chronic kidney disease. Nat. Rev. Nephrol. *7*, 286–294.

5. Kato, M., Zhang, J., Wang, M., Lanting, L., Yuan, H., Rossi, J.J., and Natarajan, R. (2007). MicroRNA-192 in diabetic kidney glomeruli and its function in TGF-beta-induced collagen expression via inhibition of E-box repressors. Proc. Natl. Acad. Sci. USA *104*, 3432–3437.

6. Lai, J.Y., Luo, J., O'Connor, C., Jing, X., Nair, V., Ju, W., Randolph, A., Ben-Dov, I.Z., Matar, R.N., Briskin, D., et al. (2015). MicroRNA-21 in glomerular injury. J. Am. Soc. Nephrol. *26*, 805–816.

7. Gomez, I.G., MacKenna, D.A., Johnson, B.G., Kaimal, V., Roach, A.M., Ren, S., Nakagawa, N., Xin, C., Newitt, R., Pandya, S., et al. (2015). Anti-microRNA-21 oligonucleotides prevent Alport nephropathy progression by stimulating metabolic pathways. J. Clin. Invest. *125*, 141–156.

8. Osipova, J., Fischer, D.C., Dangwal, S., Volkmann, I., Widera, C., Schwarz, K., Lorenzen, J.M., Schreiver, C., Jacoby, U., Heimhalt, M., et al. (2014). Diabetes-associated microRNAs in pediatric patients with type 1 diabetes mellitus: a cross-sectional cohort study. J. Clin. Endocrinol. Metab. *99*, E1661–E1665.

9. Yamamoto, T., Nakamura, T., Noble, N.A., Ruoslahti, E., and Border, W.A. (1993). Expression of transforming growth factor beta is elevated in human and experimental diabetic nephropathy. Proc. Natl. Acad. Sci. USA *90*, 1814–1818.

10. Wolf, G., Sharma, K., Chen, Y., Ericksen, M., and Ziyadeh, F.N. (1992). High glucose-induced proliferation in mesangial cells is reversed by autocrine TGF-beta. Kidney Int. *42*, 647–656.

11. Hoffmann, I., Draetta, G., and Karsenti, E. (1994). Activation of the phosphatase activity of human cdc25A by a cdk2-cyclin E dependent phosphorylation at the G1/S transition. EMBO J. *13*, 4302–4310.

12. Lukas, J., Bartkova, J., and Bartek, J. (1996). Convergence of mitogenic signalling cascades from diverse classes of receptors at the cyclin D-cyclin-dependent kinase-pRb-controlled G1 checkpoint. Mol. Cell. Biol. *16*, 6917–6925.

13. Lorenzen, J.M., Schauerte, C., Hübner, A., Kölling, M., Martino, F., Scherf, K., Batkai, S., Zimmer, K., Foinquinos, A., Kaucsar, T., et al. (2015). Osteopontin is indispensible for AP1-mediated angiotensin II-related miR-21 transcription during cardiac fibrosis. Eur. Heart J. *36*, 2184–2196.

14. Wolf, G., Chen, S., and Ziyadeh, F.N. (2005). From the periphery of the glomerular capillary wall toward the center of disease: podocyte injury comes of age in diabetic nephropathy. Diabetes *54*, 1626–1634.

15. Nadarajah, R., Milagres, R., Dilauro, M., Gutsol, A., Xiao, F., Zimpelmann, J., Kennedy, C., Wysocki, J., Batlle, D., and Burns, K.D. (2012). Podocyte-specific overexpression of human angiotensin-converting enzyme 2 attenuates diabetic nephropathy in mice. Kidney Int. *82*, 292–303.

16. Putta, S., Lanting, L., Sun, G., Lawson, G., Kato, M., and Natarajan, R. (2012). Inhibiting microRNA-192 ameliorates renal fibrosis in diabetic nephropathy. J. Am. Soc. Nephrol. *23*, 458–469.

17. Lin, C.L., Lee, P.H., Hsu, Y.C., Lei, C.C., Ko, J.Y., Chuang, P.C., Huang, Y.T., Wang, S.Y., Wu, S.L., Chen, Y.S., et al. (2014). MicroRNA-29a promotion of nephrin acetylation ameliorates hyperglycemia-induced podocyte dysfunction. J. Am. Soc. Nephrol. *25*, 1698–1709.

18. Chen, H.Y., Zhong, X., Huang, X.R., Meng, X.M., You, Y., Chung, A.C., and Lan, H.Y. (2014). MicroRNA-29b inhibits diabetic nephropathy in db/db mice. Mol. Ther. *22*, 842–853.

19. Wang, B., Komers, R., Carew, R., Winbanks, C.E., Xu, B., Herman-Edelstein, M., Koh, P., Thomas, M., Jandeleit-Dahm, K., Gregorevic, P., et al. (2012). Suppression of microRNA-29 expression by TGF-β1 promotes collagen expression and renal fibrosis. J. Am. Soc. Nephrol. *23*, 252–265.

20. Wang, B., Jha, J.C., Hagiwara, S., McClelland, A.D., Jandeleit-Dahm, K., Thomas, M.C., Cooper, M.E., and Kantharidis, P. (2014). Transforming growth factor-β1-mediated renal fibrosis is dependent on the regulation of transforming growth factor receptor 1 expression by let-7b. Kidney Int. *85*, 352–361.

21. Park, J.T., Kato, M., Lanting, L., Castro, N., Nam, B.Y., Wang, M., Kang, S.W., and Natarajan, R. (2014). Repression of let-7 by transforming growth factor-β1-induced Lin28 upregulates collagen expression in glomerular mesangial cells under diabetic conditions. Am. J. Physiol. Renal Physiol. *307*, F1390–F1403.

22. Park, J.T., Kato, M., Yuan, H., Castro, N., Lanting, L., Wang, M., and Natarajan, R. (2013). FOG2 protein down-regulation by transforming growth factor-β1-induced microRNA-200b/c leads to Akt kinase activation and glomerular mesangial hypertrophy related to diabetic nephropathy. J. Biol. Chem. *288*, 22469–22480.

23. Wang, B., Koh, P., Winbanks, C., Coughlan, M.T., McClelland, A., Watson, A., Jandeleit-Dahm, K., Burns, W.C., Thomas, M.C., Cooper, M.E., and Kantharidis, P. (2011). miR-200a Prevents renal fibrogenesis through repression of TGF-β2 expression. Diabetes *60*, 280–287.

24. Dey, N., Das, F., Mariappan, M.M., Mandal, C.C., Ghosh-Choudhury, N., Kasinath, B.S., and Choudhury, G.G. (2011). MicroRNA-21 orchestrates high glucose-induced signals to TOR complex 1, resulting in renal cell pathology in diabetes. J. Biol. Chem. *286*, 25586–25603.

25. McClelland, A.D., Herman-Edelstein, M., Komers, R., Jha, J.C., Winbanks, C.E., Hagiwara, S., Gregorevic, P., Kantharidis, P., and Cooper, M.E. (2015). miR-21 promotes renal fibrosis in diabetic nephropathy by targeting PTEN and SMAD7. Clin. Sci. *129*, 1237–1249.

26. Chau, B.N., Xin, C., Hartner, J., Ren, S., Castano, A.P., Linn, G., Li, J., Tran, P.T., Kaimal, V., Huang, X., et al. (2012). MicroRNA-21 promotes fibrosis of the kidney by silencing metabolic pathways. Sci. Transl. Med. *4*, 121ra18.

27. Thum, T., Gross, C., Fiedler, J., Fischer, T., Kissler, S., Bussen, M., Galuppo, P., Just, S., Rottbauer, W., Frantz, S., et al. (2008). MicroRNA-21 contributes to myocardial disease by stimulating MAP kinase signalling in fibroblasts. Nature *456*, 980–984.

28. Zhong, X., Chung, A.C., Chen, H.Y., Dong, Y., Meng, X.M., Li, R., Yang, W., Hou, F.F., and Lan, H.Y. (2013). miR-21 is a key therapeutic target for renal injury in a mouse model of type 2 diabetes. Diabetologia *56*, 663–674.

29. Zhong, X., Chung, A.C., Chen, H.Y., Meng, X.M., and Lan, H.Y. (2011). Smad3-mediated upregulation of miR-21 promotes renal fibrosis. J. Am. Soc. Nephrol. *22*, 1668–1681.

30. Wolf, G. (2002). Molecular mechanisms of diabetic mesangial cell hypertrophy: a proliferation of novel factors. J. Am. Soc. Nephrol. *13*, 2611–2613.

31. Kanwar, Y.S., Wada, J., Sun, L., Xie, P., Wallner, E.I., Chen, S., Chugh, S., and Danesh, F.R. (2008). Diabetic nephropathy: mechanisms of renal disease progression. Exp. Biol. Med. (Maywood) *233*, 4–11.

32. Wolf, G., and Shankland, S.J. (2003). P27Kip1: the "rosebud" of diabetic nephropathy? J. Am. Soc. Nephrol. *14*, 819–822.

33. Wang, P., Zou, F., Zhang, X., Li, H., Dulak, A., Tomko, R.J., Jr., Lazo, J.S., Wang, Z., Zhang, L., and Yu, J. (2009). microRNA-21 negatively regulates Cdc25A and cell cycle progression in colon cancer cells. Cancer Res. *69*, 8157–8165.

34. Abdel-Wahab, N., Weston, B.S., Roberts, T., and Mason, R.M. (2002). Connective tissue growth factor and regulation of the mesangial cell cycle: role in cellular hypertrophy. J. Am. Soc. Nephrol. *13*, 2437–2445.

35. Nagai, K., Matsubara, T., Mima, A., Sumi, E., Kanamori, H., Iehara, N., Fukatsu, A., Yanagita, M., Nakano, T., Ishimoto, Y., et al. (2005). Gas6 induces Akt/mTOR-mediated mesangial hypertrophy in diabetic nephropathy. Kidney Int. *68*, 552–561.

36. Sekizuka, K., Tomino, Y., Sei, C., Kurusu, A., Tashiro, K., Yamaguchi, Y., Kodera, S., Hishiki, T., Shirato, I., and Koide, H. (1994). Detection of serum IL-6 in patients with diabetic nephropathy. Nephron *68*, 284–285.

37. Suzuki, D., Miyazaki, M., Naka, R., Koji, T., Yagame, M., Jinde, K., Endoh, M., Nomoto, Y., and Sakai, H. (1995). In situ hybridization of interleukin 6 in diabetic nephropathy. Diabetes *44*, 1233–1238.

38. Lin, J.S., Shi, Y., Peng, H., Shen, X., Thomas, S., Wang, Y., Truong, L.D., Dryer, S.E., Hu, Z., and Xu, J. (2015). Loss of PTEN promotes podocyte cytoskeletal rearrangement, aggravating diabetic nephropathy. J. Pathol. *236*, 30–40.

39. Xing, L., Liu, Q., Fu, S., Li, S., Yang, L., Liu, S., Hao, J., Yu, L., and Duan, H. (2015). PTEN Inhibits High Glucose-Induced Phenotypic Transition in Podocytes. J. Cell. Biochem. *116*, 1776–1784.

40. Obad, S., dos Santos, C.O., Petri, A., Heidenblad, M., Broom, O., Ruse, C., Fu, C., Lindow, M., Stenvang, J., Straarup, E.M., et al. (2011). Silencing of microRNA families by seed-targeting tiny LNAs. Nat. Genet. *43*, 371–378.

41. Gebeshuber, C.A., Kornauth, C., Dong, L., Sierig, R., Seibler, J., Reiss, M., Tauber, S., Bilban, M., Wang, S., Kain, R., et al. (2013). Focal segmental glomerulosclerosis is induced by microRNA-193a and its downregulation of WT1. Nat. Med. *19*, 481–487.

42. Lorenzen, J.M., Kaucsar, T., Schauerte, C., Schmitt, R., Rong, S., Hübner, A., Scherf, K., Fiedler, J., Martino, F., Kumarswamy, R., et al. (2014). MicroRNA-24 antagonism prevents renal ischemia reperfusion injury. J. Am. Soc. Nephrol. *25*, 2717–2729.

43. Dong, Z., Lavrovsky, V., and Colburn, N.H. (1995). Transformation reversion induced in JB6 RT101 cells by AP-1 inhibitors. Carcinogenesis *16*, 749–756.

44. Sharma, A., Yun, H., Jyotsana, N., Chaturvedi, A., Schwarzer, A., Yung, E., Lai, C.K., Kuchenbauer, F., Argiropoulos, B., Görlich, K., et al. (2015). Constitutive IRF8 expression inhibits AML by activation of repressed immune response signaling. Leukemia *29*, 157–168.

YMTHE, Volume *25*

Supplemental Information

Therapeutic miR-21 Silencing Ameliorates Diabetic Kidney Disease in Mice

Malte Kölling, Tamas Kaucsar, Celina Schauerte, Anika Hübner, Angela Dettling, Joon-Keun Park, Martin Busch, Xaver Wulff, Matthias Meier, Kristian Scherf, Nóra Bukosza, Gábor Szénási, Mária Godó, Amit Sharma, Michael Heuser, Peter Hamar, Claudia Bang, Hermann Haller, Thomas Thum, and Johan M. Lorenzen

Figure S1

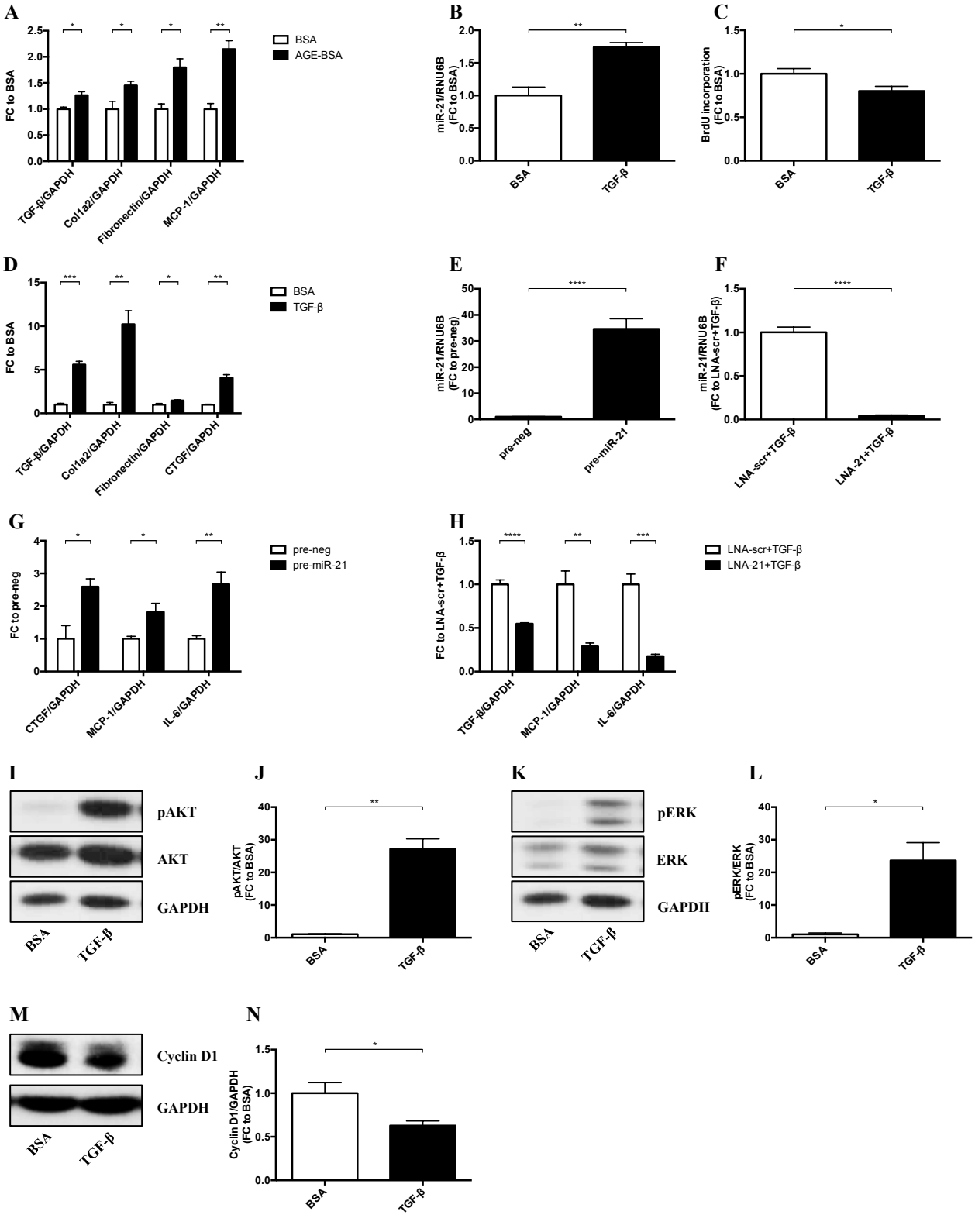
A
FC to BSA
BSA
AGE-BSA
TGF-β/GAPDH
Col1a2/GAPDH
Fibronectin/GAPDH
MCP-1/GAPDH
B
miR-21/RNU6B (FC to BSA)
BSA
TGF-β
C
BrdU incorporation (FC to BSA)
BSA
TGF-β
D
FC to BSA
BSA
TGF-β
TGF-β/GAPDH
Col1a2/GAPDH
Fibronectin/GAPDH
CTGF/GAPDH
E
miR-21/RNU6B (FC to pre-neg)
pre-neg
pre-miR-21
F
miR-21/RNU6B (FC to LNA-scr+TGF-β)
LNA-scr+TGF-β
LNA-21+TGF-β
G
FC to pre-neg
pre-neg
pre-miR-21
CTGF/GAPDH
MCP-1/GAPDH
IL-6/GAPDH
H
FC to LNA-scr+TGF-β
LNA-scr+TGF-β
LNA-21+TGF-β
TGF-β/GAPDH
MCP-1/GAPDH
IL-6/GAPDH
I
pAKT
AKT
GAPDH
BSA
TGF-β
J
pAKT/AKT (FC to BSA)
BSA
TGF-β
K
pERK
ERK
GAPDH
BSA
TGF-β
L
pERK/ERK (FC to BSA)
BSA
TGF-β
M
Cyclin D1
GAPDH
BSA
TGF-β
N
Cyclin D1/GAPDH (FC to BSA)
BSA
TGF-β

Figure S2

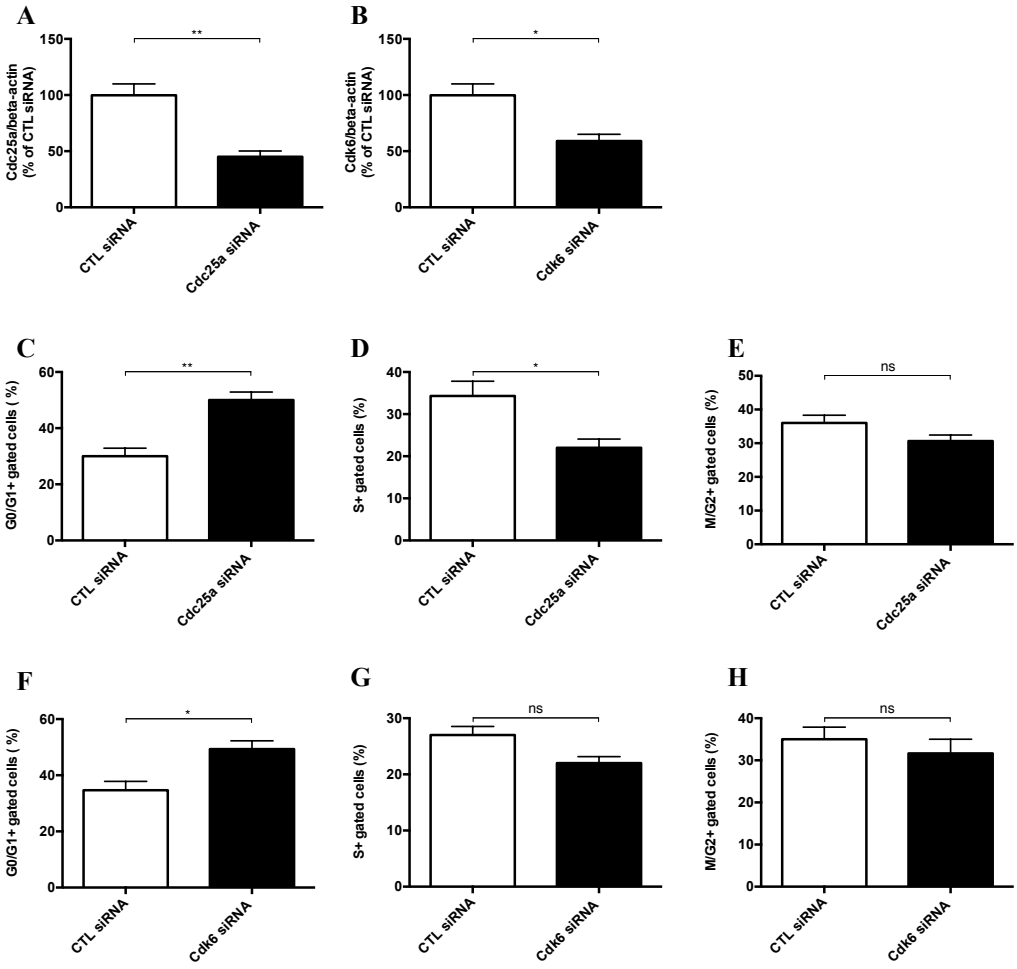
A
Cdc25a/beta-actin (% of CTL siRNA)
150
100
50
0
**
CTL siRNA
Cdc25a siRNA
B
Cdk6/beta-actin (% of CTL siRNA)
150
100
50
0
*
CTL siRNA
Cdk6 siRNA
C
G0/G1+ gated cells (%)
60
40
20
0
**
CTL siRNA
Cdc25a siRNA
D
S+ gated cells (%)
40
30
20
10
0
*
CTL siRNA
Cdc25a siRNA
E
M/G2+ gated cells (%)
50
40
30
20
10
0
ns
CTL siRNA
Cdc25a siRNA
F
G0/G1+ gated cells (%)
60
40
20
0
*
CTL siRNA
Cdk6 siRNA
G
S+ gated cells (%)
30
20
10
0
ns
CTL siRNA
Cdk6 siRNA
H
M/G2+ gated cells (%)
40
30
20
10
0
ns
CTL siRNA
Cdk6 siRNA

Figure S3

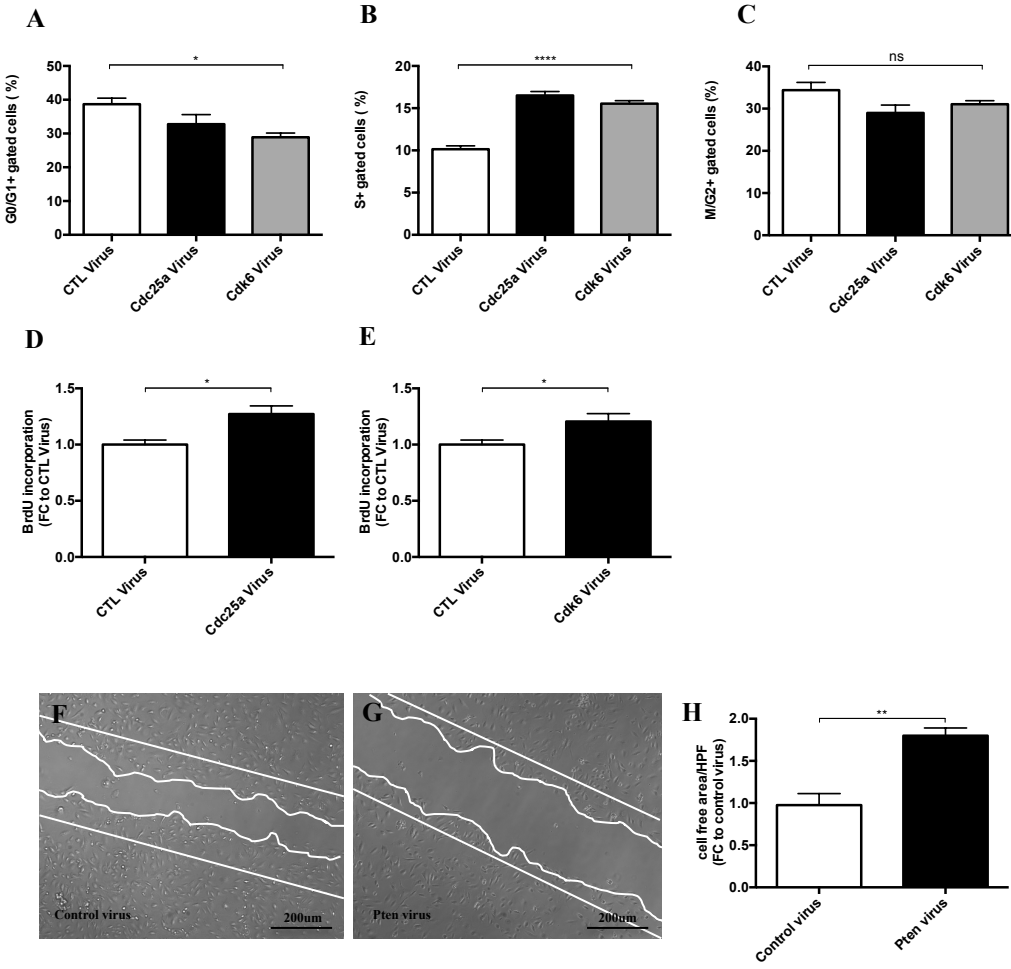
A
G0/G1+ gated cells (%)
*
CTL Virus
Cdc25a Virus
Cdk6 Virus
B
S+ gated cells (%)
****
C
M/G2+ gated cells (%)
ns
D
BrdU incorporation (FC to CTL Virus)
E
F
Control virus
200um
G
Pten virus
H
cell free area/HPF (FC to control virus)
**
Control virus
Pten virus

Figure S4

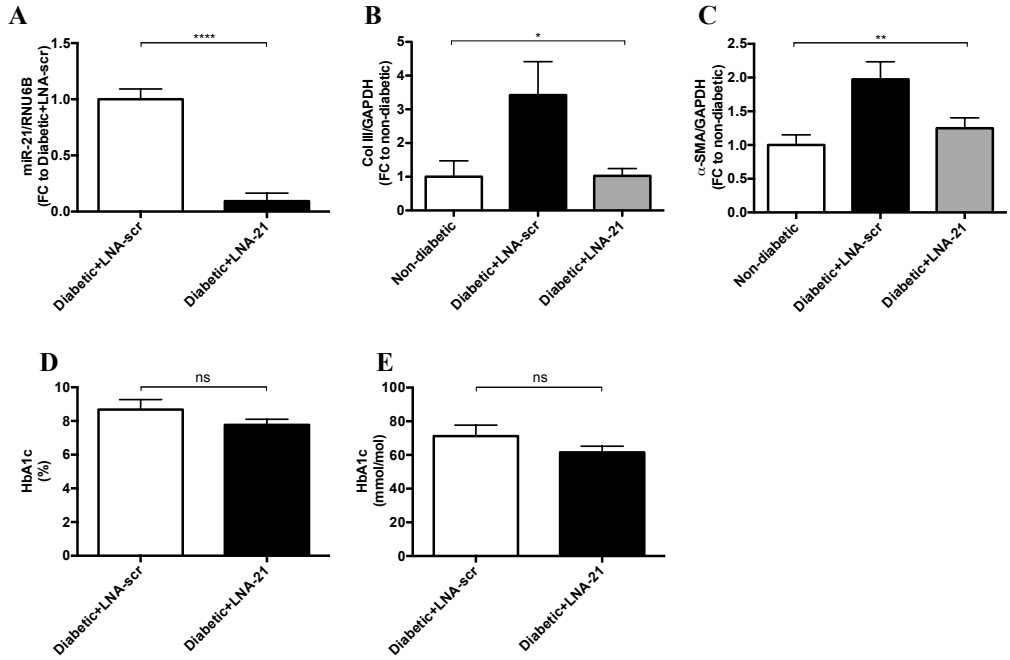
A
miR-21/RNU6B
(FC to Diabetic+LNA-scr)
****
Diabetic+LNA-scr
Diabetic+LNA-21
B
Col III/GAPDH
(FC to non-diabetic)
*
Non-diabetic
Diabetic+LNA-scr
Diabetic+LNA-21
C
α-SMA/GAPDH
(FC to non-diabetic)
**
Non-diabetic
Diabetic+LNA-scr
Diabetic+LNA-21
D
HbA1c
(%)
ns
Diabetic+LNA-scr
Diabetic+LNA-21
E
HbA1c
(mmol/mol)
ns
Diabetic+LNA-scr
Diabetic+LNA-21

Figure S5

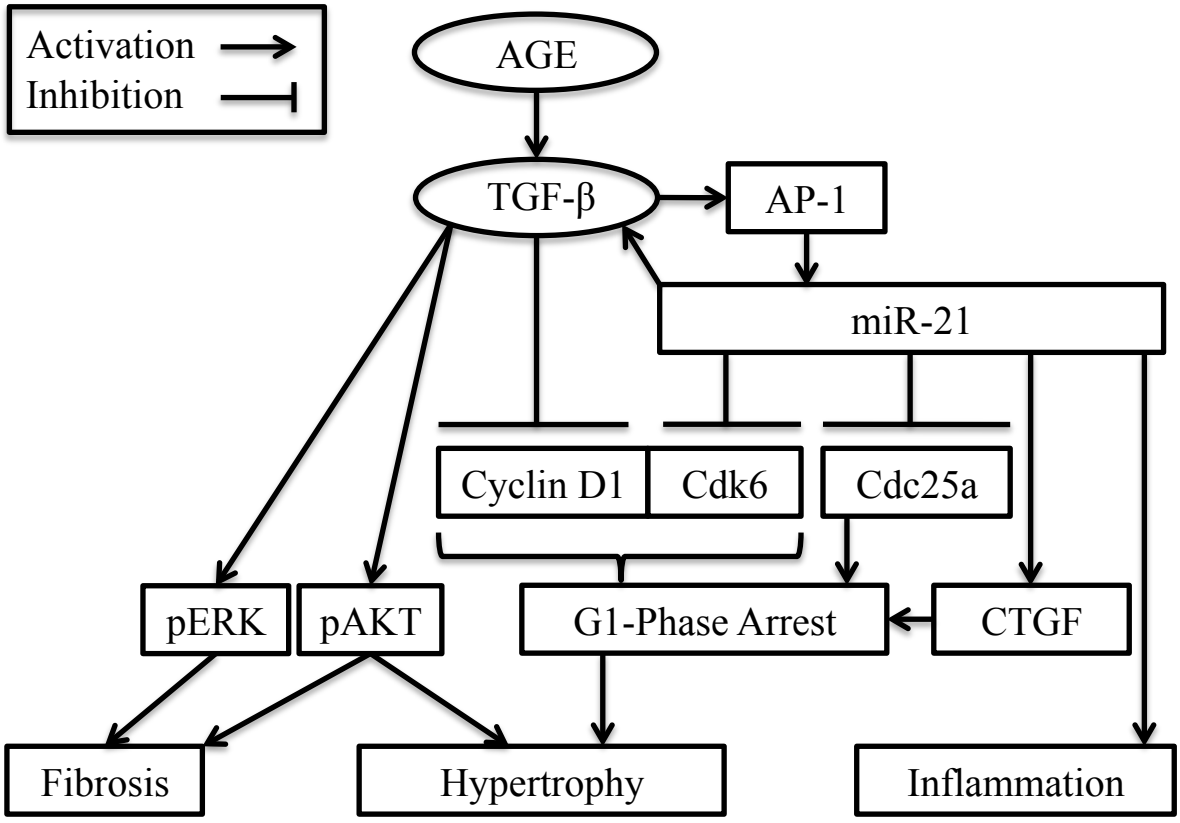
Activation
Inhibition
AGE
TGF-β
AP-1
miR-21
Cyclin D1
Cdk6
Cdc25a
pERK
pAKT
G1-Phase Arrest
CTGF
Fibrosis
Hypertrophy
Inflammation

Supplemental Figure Legends

Figure S1: MiR-21 promotes inflammatory and pro-fibrotic processes in mesangial cells. qPCR quantifications of TGF-β, Col1a2-, Fibronectin- and MCP-1 gene expression after treating mesangial cells with advanced glycation end products (A) (n=4). qPCR quantification of miR-21 (B) (n=4). BrdU incorporation in mesangial cells after TGF-β treatment (C) (n=6). qPCR quantifications of TGF-β, Col1a2, Fibronectin and CTGF (n=3) after TGFβ treatment (D). Efficacy of pre-miR-21/pre-neg transfection (E) (n=5) and LNA-21/LNA-scr (n=4) transfection with additional TGF-β treatment (F) by qPCR quantification of miR-21. qPCR quantification of CTGF, MCP-1 and Il-6 after overexpression of miR-21 (G) (n=3). qPCR quantification of TGF-β, MCP-1 and Il-6 after TGF-β treatment upon miR-21 silencing (H) (n=3). Western Blot analysis of AKT phosphorylation (I-J), ERK phosphorylation (K-L), and protein expression of Cyclin D1 (M-N) after TGF-β treatment (n=3). *P<0.05; **P<0.01; ***P<0.001; ****P<0.0001.

Figure S2: Knockdown efficacy of Cdc25a- (A) and Cdk6 (B) siRNA (n=4). Quantification of mesangial cells detected in G0/G1-phase, S-phase and M/G2-phase after liposomal transfection of siRNA silencing either Cdc25a (C-E) or Cdk6 (F-H) compared to control siRNA, respectively (n=3). *P<0.05; **P<0.01; ***P<0.001; ****P<0.0001.

Figure S3: Quantification of mesangial cells detected in G0/G1-phase, S-phase and M/G2-phase after adenoviral overexpression of Cdc25a and Cdk6 compared to Beta-Gal control virus, respectively (A-C) (n=4). BrdU incorporation in mesangial cells after adenoviral overexpression of Cdc25a and Cdk6 compared to Beta-Gal control virus, respectively (D-E) (n=4). Scratch Migration for 8h in podocytes with viral overexpression of Pten compared to viral overexpression of control (F-G); quantification of the cell free area after 8h migration (H) (n=4). *P<0.05; **P<0.01; ***P<0.001; ****P<0.0001.

Figure S4: Therapeutic efficacy of miR-21 inhibition by LNA-21 in kidneys of diabetic mice (A). qPCR quantification of ColIII (B) and α-SMA (C) in kidneys of non-diabetic mice and both diabetic mice treated with LNA-scr and LNA-21. Glycated hemoglobin count (HbA1c) in % (D) and mmol/mol (E) in diabetic mice treated with LNA-21 and LNA-scrambled oligonucleotides. *P<0.05; **P<0.01; ***P<0.001; ****P<0.0001.

Figure S5: Summary of the main findings in MC. Hypertrophy, inflammation and fibrogenesis in MCs: Advanced glycation end products (AGE) upon diabetes induction result in an increase in TGF-β, thereby leading to an AP-1 dependent increase of miR-21, which in turn potentiates TGF-β. MiR-21 represses Cdc25a and Cdk6 leading to reduced G1/S phase transition. Protein production in G1-phase results in MC hypertrophy. TGF-β degrades Cyclin D1, further disturbing cell cycle progression. MiR-21 mediated CTGF induction further promotes G1-phase arrest. AKT and ERK signaling are activated by TGF-β. AKT signaling endorses MC hypertrophy. Both activated AKT and ERK signaling are involved in fibrogenesis. Enhanced levels of miR-21 provoke inflammation.

Table S1

Primer pairs used for gene expression analysis

Gene symbol	Gene name	Primer pairs
Tgfb	transforming growth factor beta [*Mus musculus*]	Fwd: CAACAATTCCTGGCGTTACCTTGG Rev: GAAAGCCCTGTATTCCGTCTCCTT
Ctgf	connective tissue growth factor [*Mus musculus*]	Fwd: CCTAGCTGCCTACCGACTG Rev: TTAGAACAGGCGCTCCACTC
Col1a2	collagen, type I, alpha 2 [*Mus musculus*]	Fwd: CAGAACATCACCTACCACTGCAA Rev: TTCAACATCGTTGGAACCCTG
Fn1	fibronectin 1 [*Mus musculus*]	Fwd: CAGACCTACCCAGGCACAAC Rev: CAGCGACCCGTAGAGGTTTT
Acta2	actin, alpha 2, smooth muscle, aorta [*Mus musculus*]	Fwd: ACTACTGCCGAGCGTGAGAT Rev: AAGGTAGACAGCGAAGCCAG
Ccl2 (MCP-1)	chemokine (C-C motif) ligand 2 (Monocyte chemoattractant protein-1) [*Mus musculus*]	Fwd: GGCTCAGCCAGATGCAGTTA Rev: ACTACAGCTTCTTTGGGACA
Il6	interleukin 6 [*Mus musculus*]	Fwd: GAGAAAAGAGTTGTGCAATG Rev: ATTTTCAATAGGCAAATTTC